Ultrasonic characterization of HCT cells in the 5-25 MHz range

by

Amy Longstreth

A thesis submitted to the Department of Physics
in partial fulfillment of the
requirements for the degree of
Bachelor of Arts in Physics

Mount Holyoke College
May 2017

Abstract

Early recognition of cancerous tissue is crucial in receiving a favorable prognosis. There is a need for fast and easy diagnosis of tumors provided in real time. Ultrasound techniques that can be used to differentiate ultrasonic characteristics (such as speed of sound (SOS), attenuation, and backscatter coefficients (BSC)) in malignant and benign cells can aid in early diagnostics. Diagnostic ultrasound is advantageous in that it is noninvasive, inexpensive, and does not employ ionizing radiation which can increase the risk of getting cancer. Although statistically significant distinctions between benign and cancerous tumor scatterer properties have been demonstrated, there is little knowledge about which cell characteristics create differences in scattering. This thesis centers on introducing a cell pellet biophantom technique that employs the use of quantitative ultrasound to quantify the microstructure of HCT (colon cancer) cells in an attempt to establish a greater understanding of scattering mechanisms.

To analyze these characteristics HCT cells were cultured, suspended in agar and prepared into samples. Broadband BSC measurements were conducted using focused transducers and narrowband attenuation and SOS measurements were performed using receiving and transmitting transducers. All experiments were made in the 5-25MHz range at 33°C. The results introduce relevant data useful for comparative studies and further analysis.

Acknowledgements

First of all, I wish to express my grateful appreciation to my research advisor, Maria Teresa Herd, for her encouragement, guidance and support throughout this investigation. Thank you for training me to do independent research and pushing me to progress above and beyond my limits as a researcher and scientist. Thank you also, for all of the wonderful baked treats and delicious dinners at your house. You have truly been a great role model and mentor and it has been such a pleasure to work with you.

I wish to thank my committee members Dr. Kathy Aidala and Dr. Maria Gomez for their suggestions and help.

I am grateful to my lab mates, Judene Thomas and Chloe Verducci for their support. Judene, thank you for working long hours into the nights performing the experiments with me and helping with cell culture. Chloe, thank you for providing me with photographs of the HCT cells under magnification.

I would also like to thank all of the professors at the Mount Holyoke Physics Department for fostering my love for physics and passion for research. I am very lucky to have been able to learn from such enthusiastic and inspirational professors.

This thesis would not exist without the continual support of my friends and family. To Maria Patterson, thank you for always lending an ear when I was struggling or wanting to give up. To my parents, thank you for always being encouraging and believing in me and thank you to my older brother Aaron and passing your wisdom down to me.

Once again, a big thank you to each and every one of you!

Table of Contents

List of Figures

List of Tables

Chapter 1

Introduction

1.1 Quantitative Ultrasound

Ultrasound is a common diagnostic technique used in medical imaging because it is relatively inexpensive, portable, noninvasive, easily accessible and has the possibility of getting real time data [1, 2]. Ultrasound imaging, also called sonography involves exposing part of the body to high-frequency sound waves to produce pictures of the inside of the body. Typical clinical ultrasound machines employ linear or phased array probes with frequencies ranging from 1 to 10 MHz to form conventional B-mode images [3]. These images are constructed by generating a gray-scale images using the envelope-detected radio frequency (RF) signals that are backscattered. Reflections from interfaces between acoustically different regions (macrostructure) and coherent and incoherent scattering from tissues (microstructures) create the RF echoes [4]. Due to its ability to display large scale structures and morphology, B-mode ultrasound imaging has gained wide acceptance in many departments such as gynecology, cardiology, oncology, and more. Ultrasound images are captured in real time, so they can show the structure and movement of the body's internal organs, as well as blood flowing through blood vessels. However, because ultrasonography is highly operator and instrument dependent, B-mode images lack quantitative information and medical diagnosis is often highly subjective [3].

To obtain qualitative ultrasound (QUS) information about the examined tissue, would require alternate ways of collecting and processing the ultrasonic RF data so that the quantitative tissue properties are independent of instrumentation and the operator. One approach is to utilize frequency-dependent of the RF data to estimate the attenuation and backscatter coefficient

(BSC), which are intrinsic properties of the tissue [1]. In the last few decades QUS methods have gained recognition as they have proved able to examine well defined regions of interest (ROI) in soft tissues and determine statistical properties of the tissue microstructures. Using QUS methods prostate cancer, ocular tumors, liver and cardiac abnormalities have been diagnosed [5,6,7,8], benign fibroadenomas and mammary carcinomas have been differentiated, [9] and prostate cancer detection and lesion localization has had good diagnostic accuracy [10].

1.2 Introduction to Colorectal Cancer

In this study, we are using QUS to characterize the acoustic properties of the HCT166 cell line. HCT116 is one of 3 strains of malignant cells isolated from a male with colonic carcinoma [11]. Colorectal cancer, otherwise known as large bowel or colon cancer begins as a growth called a polyp on the inner lining of the colon or rectum. It is the third leading cause of cancer related deaths in women in the United States and the second leading cause in men, but if caught early is one of the most treatable forms of cancer [12]. Acceptable screening tests for colorectal cancer include high-sensitivity fecal occult blood tests, stool DNA test, sigmoidoscopy and colonoscopy [13]. While these methods are safe and have been proven to be an effective way to screen for colon cancer, some patients cannot tolerate these procedures or may be at higher risk for sedation. Thus, noninvasion visualization of living tissue by using QUS at the microscopic level is a long cherished dream in the fields of medicine and biology.

1.3 The Proposed Study

The purpose of this thesis is to show that quantitative ultrasound can be used to differentiate between the microstructure of benign and malignant cells lines. In focusing on colon cancer, or

the HCT 116 cell line, we hope to show that although cancer cells are a complex scattering media, QUS has the potential to provide a tool to diagnose and classify cancerous cells with high sensitivity and specificity.

There are several approaches to characterize cell lines. We use the cell pellet technique to experimentally measure the speed of sound, or the speed at which sound travels in a given medium under specified conditions, the attenuation, a measurement of how strongly the transmitted ultrasound decreases as a function of frequency, and the backscatter a measurement of the scattering of the wave at 180° angle from the incident. We employ both frequencies used in clinical settings (5 MHz, 10 MHz and 15MHz) as well as higher frequencies (20 MHz, and 25 MHz) which are able to characterize the cells due to subcellular scatterers, such as the nucleolus.

Previous studies using the cell pellet biophantom techniques have demonstrated agreement between in experimentally measured backscatter and attenuation coefficients and theoretical measurements [14, 15]. The biophantoms consist of live cells embedded in a plasma thrombin supportive background. Both the attenuation and backscatter are shown to increase with frequency.

This thesis is organized as follows: Chapter 2 introduces basic acoustic theory and reviews the theoretical derivations leading to the equations for the attenuation and backscatter coefficient. Chapter 3 presents the experimental methods and procedures describing how the speed of sound, attenuation, and backscatter are measured in the lab and then calculated using experimental equations. It also introduces the cell culture methods and the construction of the cell pellet. Chapter 4 presents the cell concentrations for the different experiments, the attenuation results, the BSC results, and compares the BSC's RF spectrum and the planar reflector spectrum to the transducer's spectrum provided by the manufacturer. Chapter 5 discusses these results and

provides ideas for how to address the complications and limitations of the experiment. Chapter 6

introduces insight into future work and in what direction we want to take the study next.

Chapter 2

Acoustic Theory

2.1 Theoretical Basis of Attenuation Measurement

2.1.1 Attenuation, Absorption, and Scattering

Attenuation is defined as the loss of energy that an ultrasound wave experiences as it passes through a medium [16]. The energy loss of the signal is thought to arise largely from two mechanisms: absorption and the spatial redistribution of the acoustic energy wave due to scatter refraction and reflection [1,17]. Absorption is the conversion of the wave energy into heat energy. Scattering arises due to changes in compressibility and density of the medium and in figure 2.1 is shown as the redirection of the wave energy along paths that are different from the path of the incident wave. The scattered wave energy can either be absorbed or further scattered. Consider the simple scenario shown in figure 2.1, in which the ultrasound wave that is incident on a specimen is an ideal plane wave. In this scenario, the specimen is perfectly matched to the surrounding coupling medium, so the energy (represented as intensity) exiting from the specimen in the direction of the incident wave can be calculated by considering the cross-sectional area that the wave propagates through.
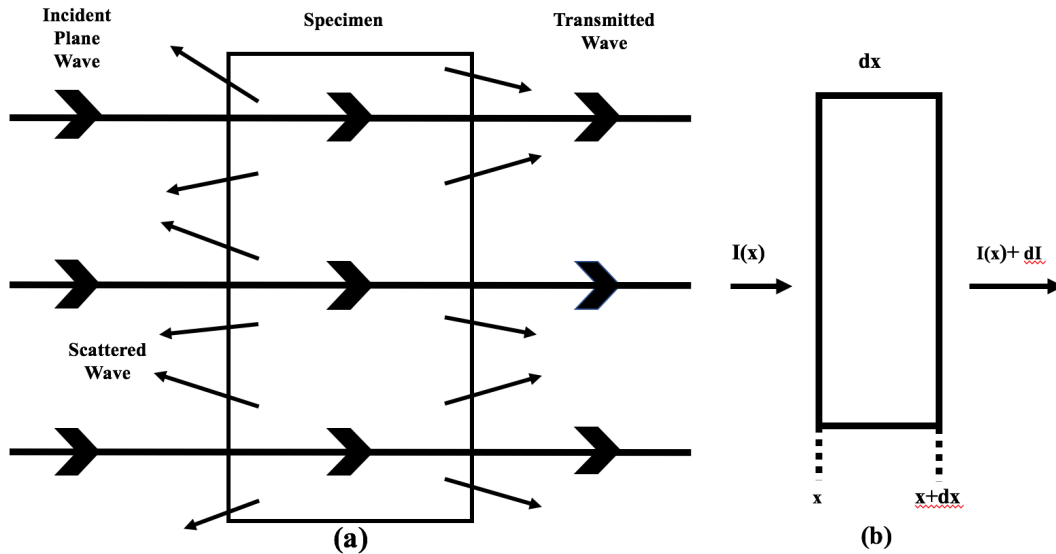
Figure 2.1: (a) Distinguishing between the absorbed, scattered, and attenuated waves passing through a specimen, and (b) change of a plane wave as a result of its passage through an incremental distance dx.

Both the absorbed and scatterer power are proportional to the time-average intensity $\bar{I}(x)$ and incremental propagation distance dx. The change in the time-average intensity due to scattering is given by the equation [16],

$$d\bar{I}_s = -\mu_s\bar{I}(x)dx \tag{2.1}$$

where μ_s is the scattering coefficient. Converting the intensity scattering coefficient into the amplitude scattering coefficient, $\mu_s = 2\alpha_s$ gives,

$$d\bar{I}_s = -2\alpha_s\,\bar{I}(x)dx. \tag{2.2}$$

Similarly, the change in time-averaged intensity due to absorption is given by

$$d\bar{I}_a = -\mu_a\bar{I}(x)dx = -2\alpha_a\,\bar{I}(x)dx \tag{2.3}$$

where μ_a is the intensity absorption coefficient and α_a is the amplitude absorption coefficient. The overall change in the time-averaged intensity due to both processes is

$$d\bar{I} = d\bar{I}_a + d\bar{I}_s = -2(\alpha_s + \alpha_a)\,\bar{I}(x)dx \tag{2.4}$$

and thus,

$$\frac{d\bar{I}}{\bar{I}(x)} = 2(\alpha_s + \alpha_a)dx. \tag{2.5}$$

By taking $\bar{I}(0)$ as the time-averaged intensity at $x = 0$, the time-averaged intensity can be found using integration at any given location x,

$$\int \frac{d\bar{I}}{\bar{I}(x)} = \int 2(\alpha_s + \alpha_a)dx \tag{2.6}$$

which gives the equation [16],

$$\bar{I}(x) = \bar{I}(0)e^{-2(\alpha_s+\alpha_a)x} = \bar{I}(0)e^{-2\alpha x} \tag{2.7}$$

where α is the amplitude attenuation coefficient and is the sum of the amplitude scattering coefficient and amplitude absorption coefficient. The amplitude of ultrasonic plane waves fall off exponentially with distance traversed though a medium. In equation 2.7, α is expressed in units of $\frac{Np}{cm}$ (α_{Np}). For experimental purposes, it is helpful to express the units in terms of $\frac{dB}{cm}$ (α_{dB}). To do so, equation 2.7 is rearranged, multiplied by 10 and then we take logarithms to the base 10,

$$10\log\left[\frac{\bar{I}(0)}{\bar{I}(x)}\right] = 20\alpha_{Np}x\log(e) = 8.686\alpha_{Np}x \tag{2.8}$$

where α_{dB} can be defined to be $8.686\alpha_{Np}$.

2.2 Theoretical Basis for Backscatter Coefficient

2.2.1 Wave Equation for an Inhomogeneous Medium

Most mediums are inhomogeneous. For example, in tissue, local variations of compressibility and density are due to the cellular nature of the medium, and these are responsible for the speckle background patterns seen in ultrasonic B-mode images. To characterize the effects of such variations, it is first necessary to obtain a wave equation

describing wave propagation in inhomogeneous mediums. In this scenario, imagine a plane wave incident on an arbitrary-shaped scattering volume with acoustic properties (density and compressibility) that can vary throughout the volume as seen in figure 2.2.

Following the derivation provided by Morse and Ingard [18] and Cobbold [16] the inhomogeneous wave equation is given by

$$\nabla^2 p - \frac{1}{c_o^2}\frac{\partial^2 p}{\partial t^2} = \frac{1}{c_o^2}\frac{\partial^2 p}{\partial t^2}\left[\frac{\kappa_v - \kappa_o}{\kappa_o}\right] + \nabla \cdot \left[\frac{\rho_v - \rho_o}{\rho_o}\nabla p\right] \tag{2.9}$$

where the left-hand side corresponds to the wave equation for a uniform medium and the right-hand side represents a radiation source due to the scattering of energy resulting from a non-uniform medium.
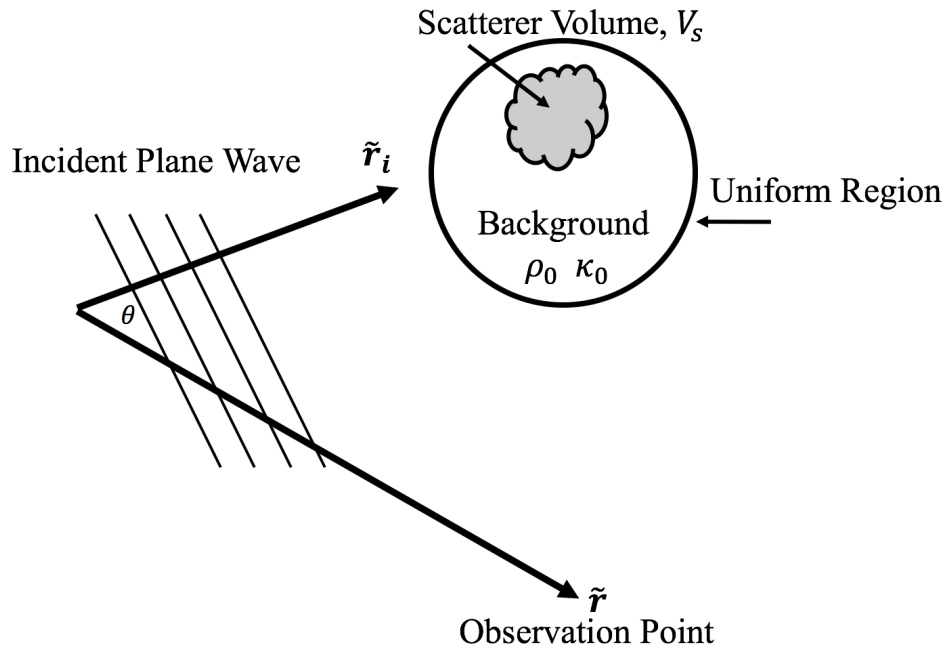
Figure 2.2: Uniform medium containing a scattering volume within which the density and compressibility vary. The unit vectors $\tilde{r}_i$ and $\tilde{r}$ are in the directions of the incident wave and observation point.

Equation 2.9 can be rewritten to obtain and integral equation that expresses the total

acoustic pressure field (incident+scattered) due to an incident wave. First, it is convenient to re-

express equation 2.9 as

$$\nabla^2 p \nabla^2 p - \frac{1}{c_0^2} \frac{\partial^2 p}{\partial t^2} = -f(\mathbf{r}: t), \qquad (2.10)$$

where the "source" term, $f(\mathbf{r}: t)$, is given by

$$f(\mathbf{r}: t) = \frac{-1}{c_0^2} \frac{\partial^2 p}{\partial t^2} \left[\frac{\kappa_v - \kappa_o}{\kappa_o} \right] - \nabla \cdot \left[\frac{\rho_v - \rho_o}{\rho_o} \nabla p \right]. \qquad (2.11)$$

Undergoing a Fourier transform equation 2.11 becomes,

$$F(\mathbf{r}: \omega) = k^2 \left[\frac{\kappa_v - \kappa_o}{\kappa_o} \right] \underline{p} - \nabla \cdot \left[\frac{\rho_v - \rho_o}{\rho_o} \nabla \underline{p} \right]. \qquad (2.12)$$

In this equation $k = \frac{\omega}{c_o}$, and is the wave number for the background medium. Using

Green's function approach to obtain an integral equation for the scattered pressure field, the

Fourier transformed version of the wave equation can be written as

$$(\nabla^2 + k^2)\underline{p} = -F(\mathbf{r}: \omega)$$

and the equation governing Green's function as

$$(\nabla^2 + k^2)G(\mathbf{r}|\mathbf{r}_o) = -\delta(\mathbf{r} - \mathbf{r}_o),$$

where G is the Green's function. After multiplying these two above equations by G and F,

subtracting, integrating over a volume V, that includes the scattering volume V_s, and using

Green's theorem, the acoustic pressure can be expressed as

$$\underline{p}(\mathbf{r}: \omega) = \int \int_s \left[G \frac{\partial \underline{p}}{\partial n} - \underline{p} \frac{\partial G}{\partial n} \right] \partial S_o + \int \int_{V_s} \int G(\mathbf{r}|\mathbf{r}_o) F(\mathbf{r}_0: \omega) dV_o. \qquad (2.13)$$

The background medium is assumed to be unbounded and thus, Green's function is $G(\mathbf{r}|\mathbf{r}_o) \equiv$

$G(|\mathbf{r} - \mathbf{r}_o|) = \frac{e^{\frac{-i\omega|\mathbf{r}-\mathbf{r}_o|}{c_o}}}{4\pi|\mathbf{r}-\mathbf{r}_o|}$. $|\mathbf{r} - \mathbf{r}_o|$ is the distance to the observation point $\mathbf{r}$ as shown in the

diagram in figure 2.3. The incident pressure wave will be equal to the incident pressure wave $\underline{p}_i$.

Using equations 2.12 and 2.13 and noting that $\underline{p}_s = \underline{p} - \underline{p}_i$ the equation for the scattered field

pressure is given,

$$\underline{p}_s(\mathbf{r}:\omega) = \int\int_{V_s}\int \left\{ k^2\underline{p}(\mathbf{r_o})\left[\frac{\kappa_v - \kappa_o}{\kappa_o}\right] G(\mathbf{r}|\mathbf{r_o}) - \nabla \cdot \left[\frac{\rho_v - \rho_o}{\rho_o}\nabla\underline{p}(\mathbf{r_o})\right] G(\mathbf{r}|\mathbf{r_o}) \right\} dV_o \quad (2.14)$$

where the operator ∇ is with respect to the coordinates of $\mathbf{r_o}$. Using the vector relation $\nabla \cdot$

$(wu) = u \cdot \nabla w + w\nabla \cdot u$, equation 2.14 can reduce to

$$\underline{p}_s(\mathbf{r}:\omega) = \int\int_{V_s}\int \left\{ k^2\underline{p}(\mathbf{r_o})\left[\frac{\kappa_v - \kappa_o}{\kappa_o}\right] G(\mathbf{r}|\mathbf{r_o}) + \left[\frac{\rho_v - \rho_o}{\rho_o}\right]\left[\nabla G(\mathbf{r}|\mathbf{r_o}) \cdot \nabla\underline{p}(\mathbf{r_o})\right] \right\} dV_o, \quad (2.15)$$

which is most commonly known as the scattering equation [16].
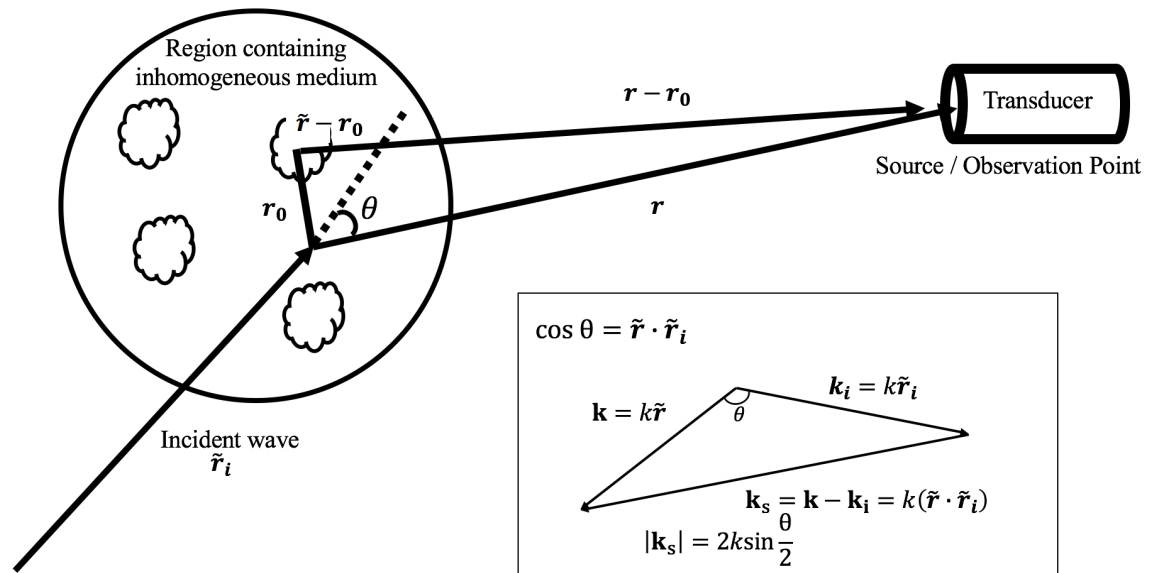
Figure 2.3: The scattering geometry of a pulse echo wave to obtain an approximate expression for Green's function in the far field. The insert shows how the scattering vector, $\mathbf{k}_s$ is related to θ. The expression for $|\mathbf{k}_s|$ was obtained by recognizing that $|\mathbf{k}_s| = k[\tilde{r}^2 + \tilde{r}_i^2 - 2(\tilde{r} \cdot \tilde{r}_i)]^{1/2} = 2k\left[\frac{1-cos\,\theta}{2}\right]^{1/2}$

2.2.2 Scattering Pressure and Scattering Amplitude in an Inhomogeneous Medium

The backscatter coefficient is defined to be the proportion of intensity scattered from an object in the direction opposite to the incident wave, or in other words, it is the differential scattering cross-section per unit volume for a scattering angle of 180° [19]. To determine the theoretical equation for backscatter, the scattering pressure and amplitude equations must first be derived from equation 2.15.

With the help of figure 2.3 Green's function can be approximated,

$$G(\mathbf{r}|\mathbf{r}_o) = \frac{e^{-ik|\mathbf{r}-\mathbf{r}_o|}}{4\pi|\mathbf{r}-\mathbf{r}_o|} \approx \frac{e^{-ik(r-\tilde{r}\cdot\tilde{r}_o)}}{4\pi},$$

where $\tilde{r}$ is a unit vector in the direction of the observation point $\mathbf{r}$. The gradient of $G(\mathbf{r}|\mathbf{r}_o)$ is approximated by,

$$\nabla G(\mathbf{r}|\mathbf{r}_o) \approx ik\tilde{r}G(\mathbf{r}|\mathbf{r}_o).$$

The incident pressure and its gradient at positon $\mathbf{r}$ for an incident plane wave in the direction of the unit vector $\tilde{r}_i$ are given by

$$\underline{p}_i = p_{im}e^{-ik(\tilde{r}_i\cdot\tilde{r})}, \nabla \underline{p}_i = -ik\tilde{r}_i\underline{p}_i,$$

where p_{im} is the pressure amplitude. Using the Born approximation, using the relationship $\cos\theta = \tilde{r}\cdot\tilde{r}_i$, and substituting the above relations into equation 2.15, the scattered pressure can be written as

$$\underline{p}_s(\mathbf{r},\tilde{r}_i) = p_{im}\frac{e^{ikr}k^2}{4\pi r}\int\int_{V_s}\int \left\{\left[\frac{\kappa_v-\kappa_o}{\kappa_o}\right] + \left[\frac{\rho_v-\rho_o}{\rho_o}\right]\cos\theta\right\}e^{-ik\tilde{r}_o\cdot(\tilde{r}-\tilde{r}_i)}dV_o. \tag{2.16}$$

From equation 2.16, the angle distribution of the scattered pressure (the scattering amplitude) can now be defined,

$$\Phi(\mathbf{k}_s) = \frac{k^2}{4\pi r}\int\int_{V_s}\int \left[\gamma_\kappa(\mathbf{r}_o)+\gamma_\rho(\mathbf{r}_o)\cos\theta\right]e^{-i\tilde{r}_o\cdot\mathbf{k}_s}dV_o \tag{2.17}$$

and the scattering pressure can be written as,

$$\underline{p}_s(\mathbf{r}, \mathbf{k}_s) = p_{im} \frac{e^{ikr}}{r} \Phi(\mathbf{k}_s). \tag{2.18}$$

Finally, the differential scattering cross-section of V_s can be obtained from equation 2.17 and the definition of the differential scattering cross-section for an incident plane wave,

$$\sigma_d(\theta, \varphi) = \frac{\text{Time Averaged Scattered Power}}{\text{Time Averaged Incident Intensity}} = \frac{d\overline{W}}{d\Omega} \frac{1}{\overline{I}} = \frac{d\sigma_s}{d\Omega},$$

where σ_s is the scattering cross-section and $d\Omega$ is an elementary solid angle. It should be noted that the differential cross-section describes the variation of the scattered power with angular direction. For this setup,

$$\sigma_d = |\Phi(\mathbf{k}_s)|^2, \tag{2.19}$$

and when measured in the 180° direction ($\sigma_d(\theta, 0)$) is called the backscattered cross-section σ_b. The backscattered coefficient is the backscattered cross-section divided by the volume,

$$\eta = \frac{|\Phi(\mathbf{k}_s)|^2}{V}, \tag{2.20}$$

and is measured in units of $\frac{1}{cm-sr}$ where sr is steradians.

Chapter 3

Materials and Methods

3.1 HCT 116 Cells

HCT 116 is a human colon cancer cell line that is commonly used to study cancer

biology. It is a growth factor independent cell line that has been shown to be invasive and highly

motile in *in vitro* studies [20,21,22]. Colon carcinoma is also the second leading cause of cancer

related deaths in the United States [23]. Unlike thyroid cancer [24], mouse tumors [25,26], and

other cancer cell lines, HCT cells have not been characterized using quantitative ultrasound. It is

for these reasons that we chose to use HCT cells in our experiments.

3.1.1 Cell Culture

Frozen HCT 116 (colon carcinoma) cells were thawed by collecting a cryogenic vial of the

cells from liquid nitrogen storage and placing only the lower half of that vial in a $37^{o}C$ water

bath. The cells thawed for 1-2 minutes until a small amount of ice remained. While thawing a

250mL culture flask (Fisher Scientific Co, Agawam MA) was labeled with the cell line name and

date. 8 mL of growth media, containing the base media McCoy's 5A medium (Sigma Aldrich,

St. Louis, MO), 9% Fetal Bovine Serum, 0.9% Penicillin Streptomycin, and 0.09% Fungizone

was pipetted into the culture flask and then the thawed cells were pipetted into the flask. The

cells were incubated at $37^{o}C$ and 5% CO_2.
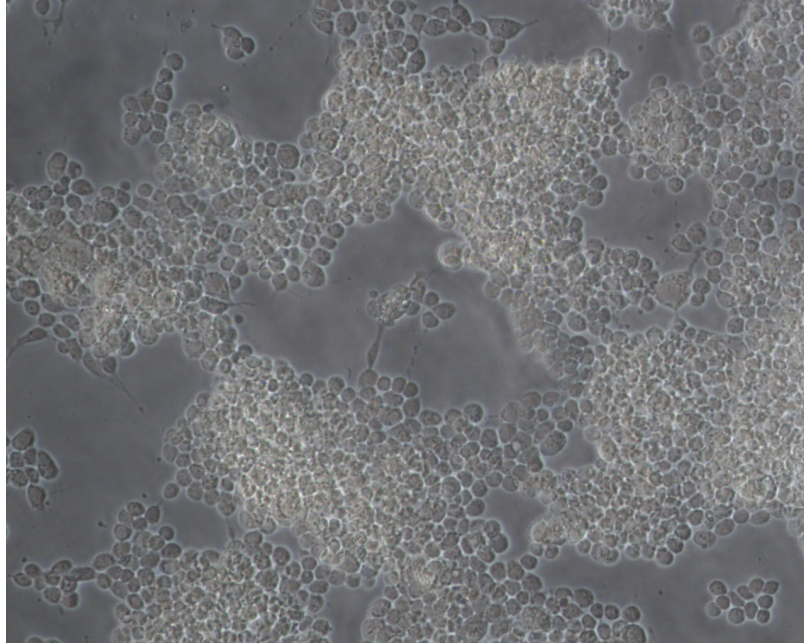
Figure 3.1: HCT cells under 10x magnification [27].

After a growing for a week the cells were examined under an inverted microscope to ensure normal growth, shown in figure 3.1, and split into four labeled 250mL cell culture flasks. First, four cell culture flasks were prepared by pipetting 7.5mL of growth into them. Next, the media in the flask containing the growing cells was discarded and the cell monolayer was washed three times with 5mL Phosphate Buffered Saline (PBS) 2mL of trypsin (Sigma Aldrich) was added to the flask containing the cells and spread around the entire bottom surface. The cells were incubated for 5-10 minutes at 37^oC and 5% CO_2. Finally, the cells were removed from the incubator and observed using an inverted microscope to ensure that the cells were no longer adhering to the flask. 8.0mL of growth medium was added to the cells and gently aspirated. 2.5 mL of the cell suspension was pipetted into the four flasks and the cultures incubated at 37^oC and 5% CO_2.

Once a week the cells were fed by removing old media and adding 8mL growth media and biweekly one flask of cells was split into four. Growth media and trypsin were pre-warmed to 37^oC but all other solutions were handled at room temperature.

3.1.2 Cell Counting

The cells were viewed using an inverted microscope to assess the degree of cell density and to confirm the absence of bacterial and fungal contaminants. Old growth media was discarded and then the cells were washed with 5mL PBS three times. After discarding the PBS, the cells were exposed to 2.0 mL trypsin for 5-10 minutes at 37^oC. At this point in time the cells appeared very loosely attached to the flask. An additional volume of fresh medium equivalent to the volume of trypsin was added to the flask and the cells were broken up through gentle pipetting. The cell solution was transferred to a centrifuge tube where $150\mu L$ was removed and added to an equal volume of trypan blue in a different centrifuge tube. The cells and trypan were mixed through gentle pipetting and vortexing. Ethanol and lens paper was used to clean the hemocytometer and the coverslip. After moistening, the coverslip was slid over the chamber using slight pressure until refraction rings appeared. Introducing the cell suspension (5-10 μL) into the V-shaped wells filled both sides of the chamber due to capillary action. The number of viable and non-viable cells were counted while viewing the hemocytometer under x40 magnification, shown in figure 3.2. The concentration of viable and nonviable cells were counted using the equations

$$\text{Viable Cells} = A * D * C \qquad\qquad (3.1)$$

and

$$\text{Nonviable Cells} = B * D * C \qquad\qquad (3.2)$$

A is the mean number of viable cells counted (total viable cells counted divided by number of squares), B is the mean number of nonviable cells counted (total nonviable cells counted divided by number of squares), C is the dilution factor (volume trypsin + volume media), and D is the correction factor (10^4 for this hemocytometer).
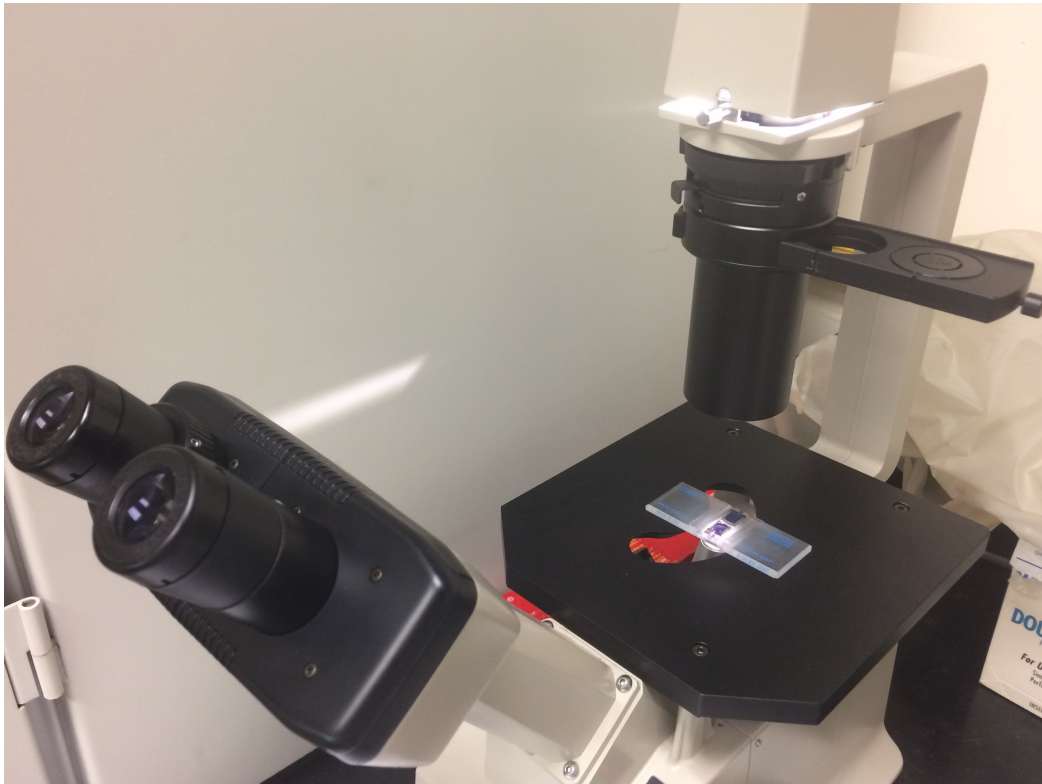
Figure 3.2: Cell counting under 40x magnification.

3.2 Cell Pellet Holder Construction

Two types of cell pellet holders of were constructed. One was made by cutting a 50mL polypropylene disposable centrifuge tube (Fisher Scientific, Agawam MA) into a hollow cylinder with a ~6mm height and ~26.5mm inside diameter. Goop adhesive was applied to one side of this cell pellet holder set glue side down on 15.1μm thick saran wrap taped to a table and

pulled tight. A weight was placed on top and the glue set for at least 24 hours, shown in figure

3.3. The other holder was fabricated by cutting 10mL polypropylene disposable centrifuge tube

(Fisher Scientific, Agawam MA) into a hollow cylinder with a ~10mm height and ~13.5mm

inside diameter, as described in figure 3.4. As this cell pellet holder is taller, it was unnecessary

to glue a saran window to one side.
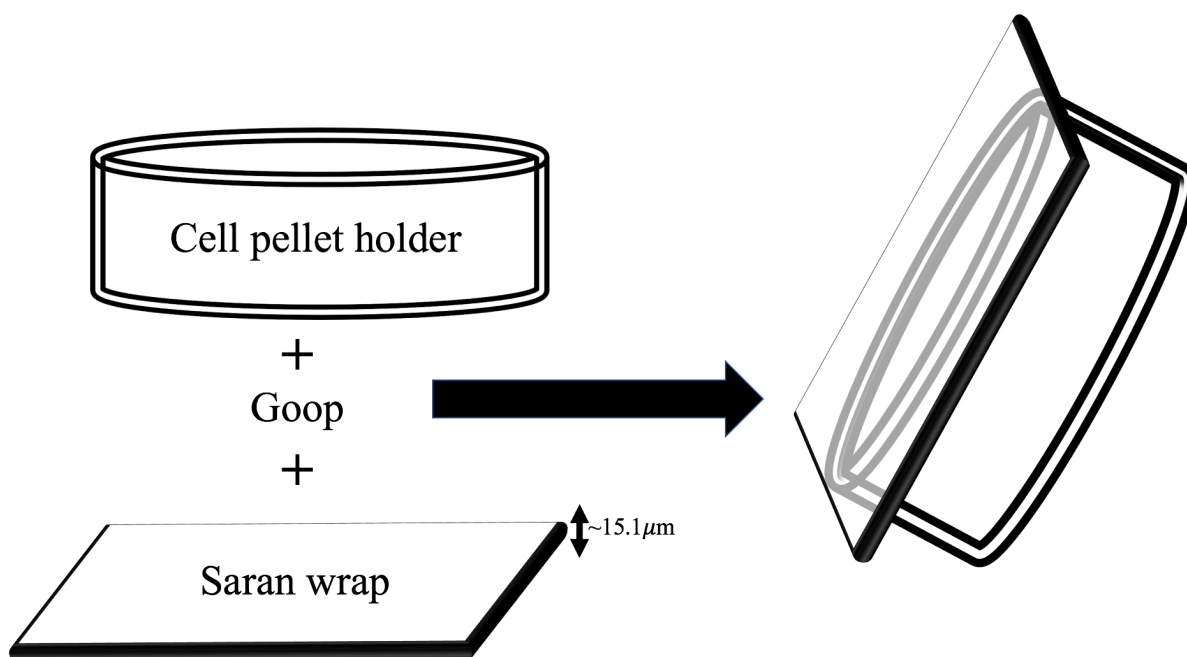
Figure 3.3: "Wide" cell pellet holder construction.
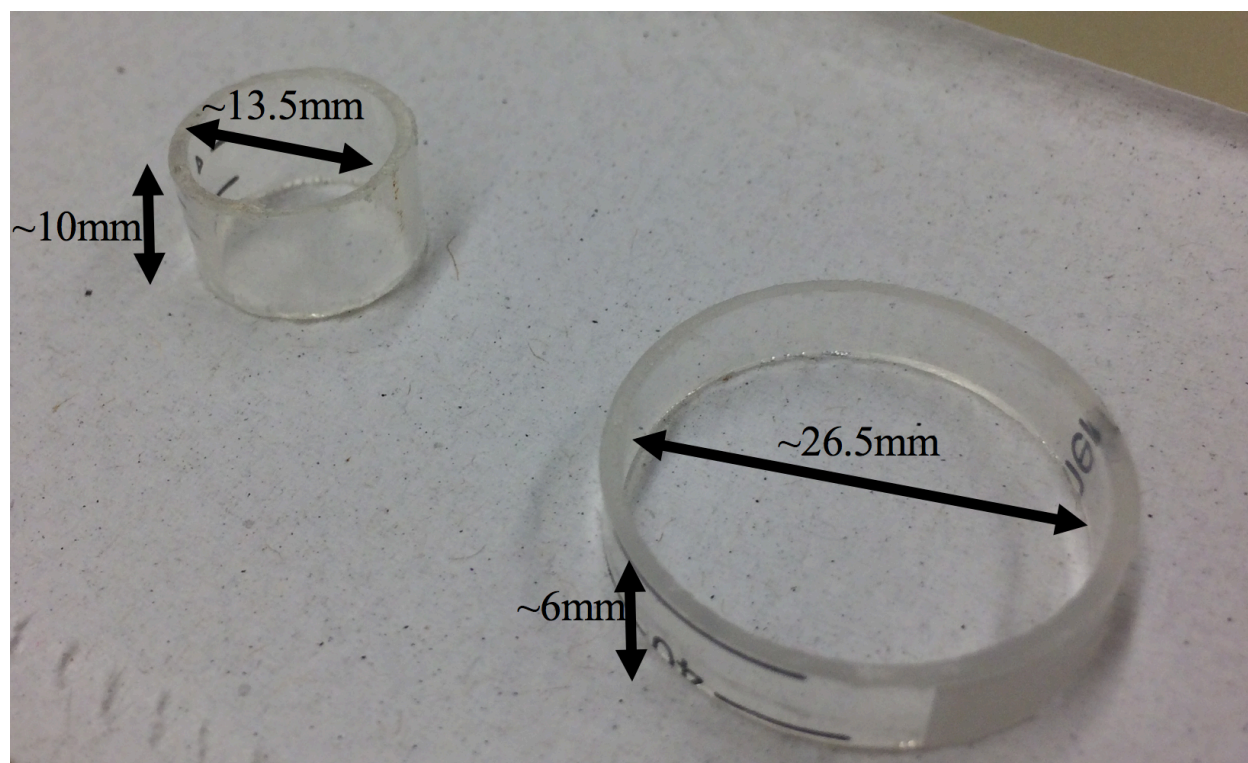
Figure 3.4: Comparison of cell holder sizes.

3.3 Cell Pellet Construction

The cell pellets were constructed by suspending live HCT cells in an agar solution. HCT (colon carcinoma) cells were cultured in McCoy's 5A growth media (3.1.1) and grown in a 250mL tissue culture flask (Fisher Scientific Co, Agawam, MA). The cell monolayer was detached from the bottom of the flask as described in previous methods (3.1.2) and subsequently pipetted into a 50mL centrifuge tube. A hemocytometer was used to count viable cells to yield the number of HCT cells per known volume. Equal volumes ($150\mu m$) of cell suspension (HCT cells in growth medium and trypsin) and the dye Trypan Blue (where it comes from) were mixed through gentle pipetting and vortexing to break up the clumps of cells. Trypan Blue was used to differentiate viable cells (bright cells) from nonviable cells (stained as blue cells). A known number of viable cells were placed into a centrifuge tube, centrifuged, and the supernatant was

removed. 1mL of 0.7% agar was added to the cell sediment in the centrifuge tube which was

then vortexed for roughly twenty seconds. The agar and cell solution was transferred to a cell

holder that had two Saran Wrap windows secured with rubber bands, shown in figure 3.5 The

media and trypsin are heated to 37 °C prior to its use and the agar is melted in a microwave but

the other materials are handled at room temperature.

Figure 3.5: Completed construction of the "wide" cell pellet.

3.4 Experimental Methods

Due to the nature of taking measurements of acoustic properties, the results of the attenuation, speed of sound and backscatter experiments can depend heavily on temperature. Temperature stability across the experiments is very important. We aim to keep the temperature of the internal setup stable by performing all of our experiments in a deionized water tank, with water temperature held steady at 33°C.

We ran all experiments with different types of transducers (unfocused for attenuation and speed of sound and focused for backscatter), of 5MHz, 10MHz, 15MHz, 20MHz, and 25MHz frequencies.

3.4.1 Speed of sound and Attenuation Experimental Setup

The speed of sound and attenuation experiment are conducted using a through transmission technique. Two transducers, one receiving and one transmitting are held in a plastic housing, shown in figure 3.6, and are fixed using two small screws. The cell pellet with the wider diameter held in a portable stand and secured using a small screw is placed between the two transducers inside a tank filled with deionized water. For this experiment the wider cell pellet is used because the receiving and transmitting transducers are unfocused and therefore have a wider beam width.
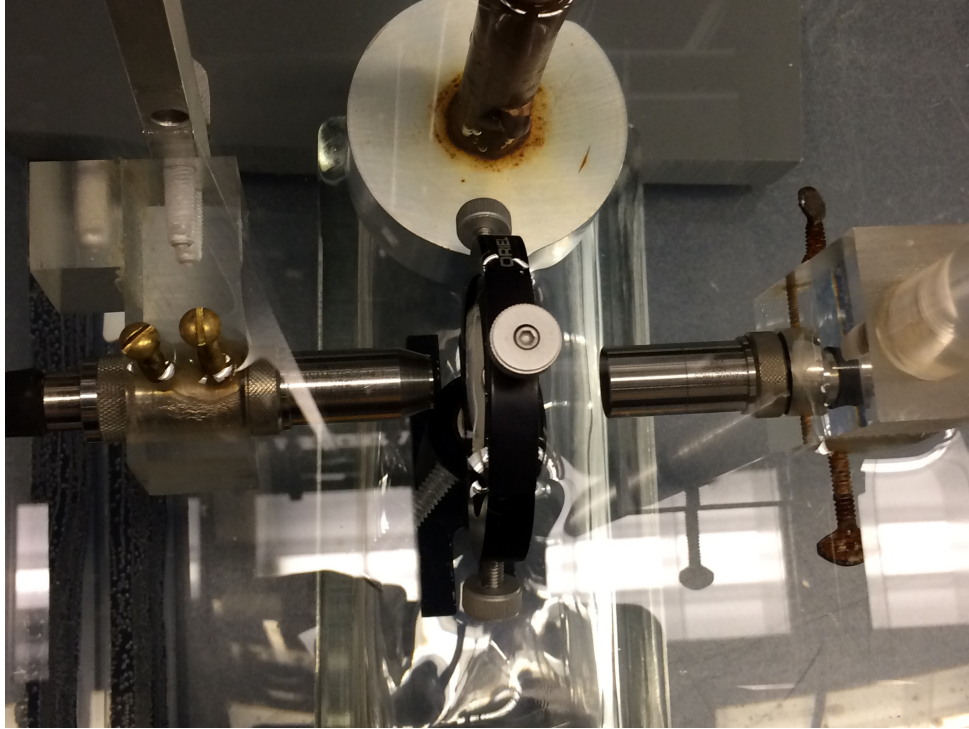
Figure 3.6: Laboratory speed of sound and attenuation setup.

It is important to ensure that the piezoelectric surfaces of the transducers are parallel. We can ensure that this is true by adjusting the angles of the transducers and noting the amplitude of the waveform on the oscilloscope. It is expected that the resultant signal may change in time (if we tilt transducer up or down), but if the amplitude of the waveform decreases then it is likely that the piezoelectric surface of the transducers is not parallel. It is necessary to realign the setup until the amplitude of the waveform is at a maximum.

A further test of alignment was done using a computer program, COSMOS, which controls a high precision x-y-z stepper motor as seen in figure 3.7. Within this program, there are two modes that can move the transducers in the x, y or z directions; a Virtual Jog, and a Quick Move, both of which can be used as a single axis movement. The translator motors correspond to a number from 1 to 3 where the number corresponds to the axis of movement. 1 represents the x-axis, 2 the y-axis, and 3 the z-axis. Using the Virtual Jog mode, the transducers were

electronically moved up and down, along the z-axis and left and right, along the y-axis, by slight amounts to see the change in amplitude. We adjusted the transducers until the resultant signal's amplitude was at its maximum.
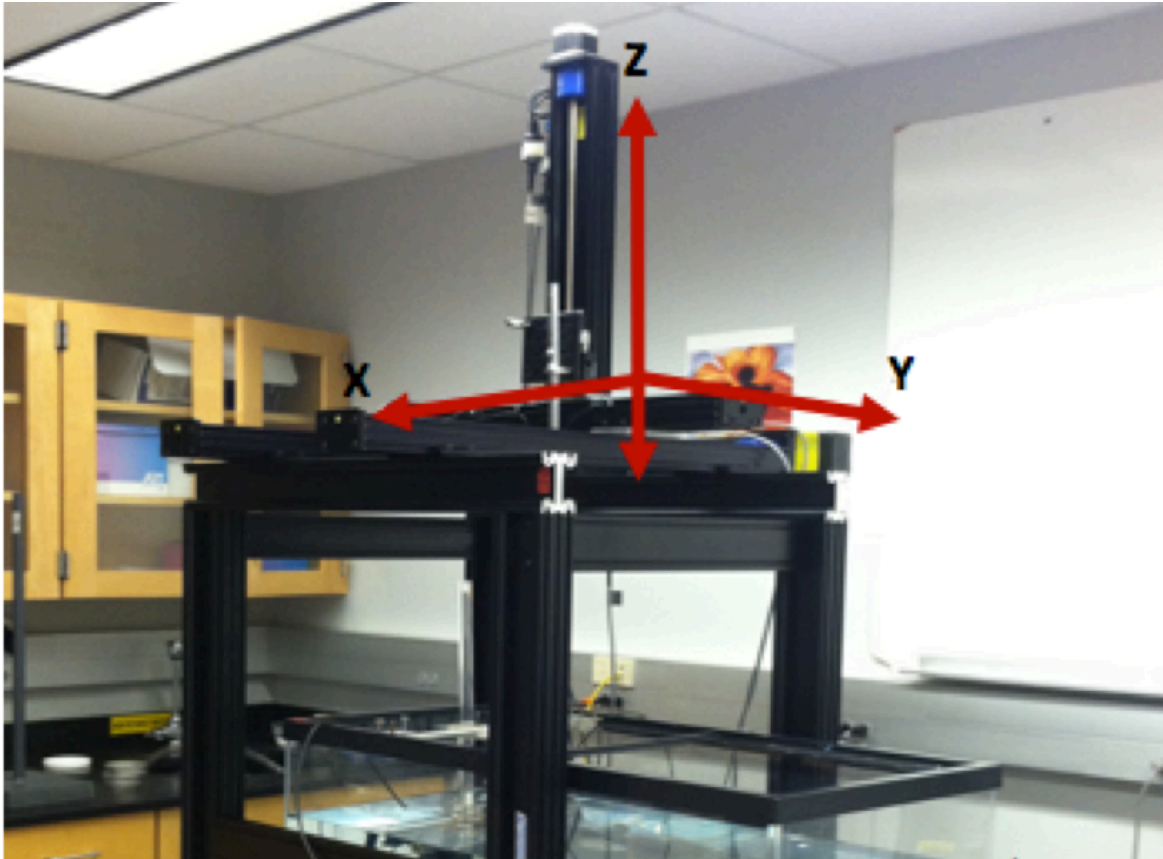
Figure 3.7: COSMOS x-y-z translator.

3.4.2 Speed of Sound and Attenuation Electronic Setup

For data collection, we used an Olympus Parametric-NDT RF power amplifier, Agilent 33500B waveform generator and a Tektronix TDS 3014C digital phosphor oscilloscope with 1.25 GS/s digitalization. The waveform generator served to excite the emitting transducer by sending out 20 short voltage cycle bursts which were then amplified by the RF power amplifier. The amplified voltage bursts were then sent to an emitting transducer which transformed the

voltage bursts into an ultrasonic pulse. The ultrasonic pulses passed through the sample and water and were received by the receiving transducer.

The emitting transducer was directly attached to the output port of the RF power amplifier using a BNC cable. The receiving transducer was connected to Channel 1 of the oscilloscope also using a BNC cable. Both transducers were connected to the cable through a mounting bracket of a male UHF adaptor. The sync out of the waveform generator was fed into the external trigger of the oscilloscope and the output of the waveform generator was linked to the input of the RF power amplifier. This electronic setup is diagramed in figure 3.8.
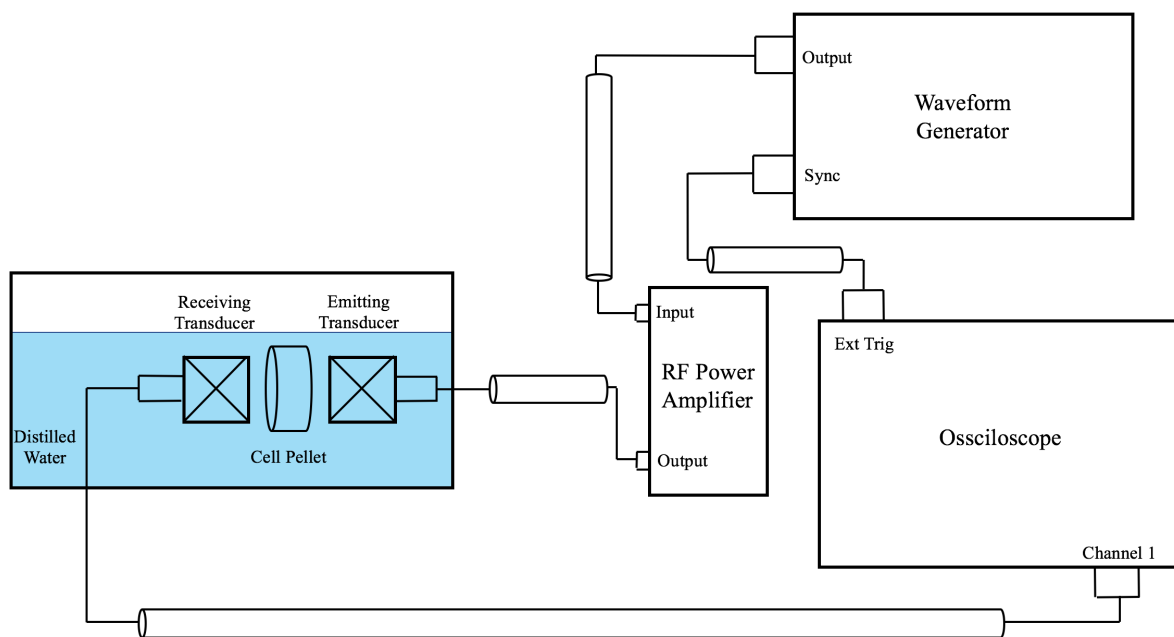
Figure 3.8: Electronic speed of sound and attenuation setup.

3.4.3 Speed of Sound Experimental Calculation

After the transducers are carefully aligned, the time it takes for the ultrasonic signal to travel through just the water (as seen on the oscilloscope) is recorded. The cell pellet is then meticulously placed in between the receiving and emitting transducers making sure that its

surfaces are parallel to the piezoelectric surfaces of both transducers and the time of propagation of the signal through the pellet is recorded, as shown in figure 3.9, where T_w is the time for the signal to travel though just the water and T_s is the time for the signal to travel though the pellet.
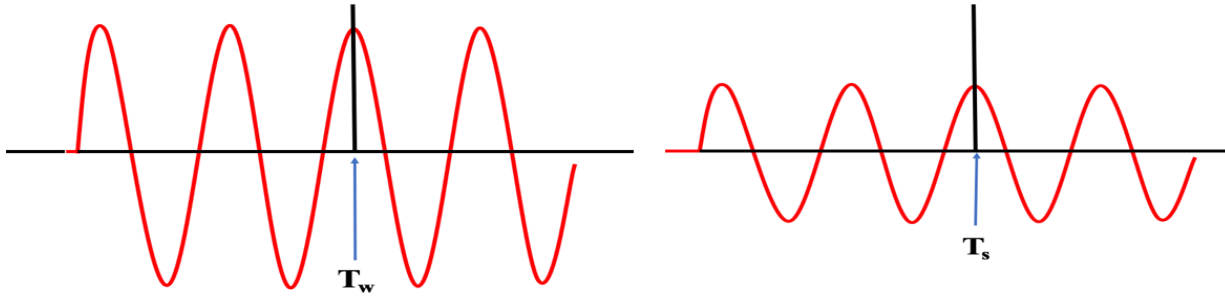
Figure 3.9: Comparison of speed of sound through the water and through the sample

This process was repeated 3-5 times to get an overall average of the speeds of sounds through both mediums. To be sure that the time was being recorded at the same distance for both the water and the pellet, the peaks of the waveforms were counted and the time was measured at the same peak. As seen in figure 3.9, both T_w and T_s are recorded on the third peak. The equation for determining the speed of sound is given by

$$C_s = \frac{1 + C_w}{C_w * \frac{\Delta t}{W_s}}$$

(3.3)

where $\Delta t = T_s - T_w$, d is the thickness of the sample, C_w is the speed of sound in water ($\approx 1516 \; m/s$)

3.4.4 Attenuation Experimental Calculation

The attenuation coefficient depends on the amplitudes of both the ultrasonic signal propagating through just the water and the ultrasonic signal propagating though the cell pellet. The amplitudes of the signals were measured in a similar manner to that of the time in section 3.5.3 and is shown in figure 3.1, where A_w is the amplitude the water only path, and A_s is the amplitude of the cell pellet path. Both A_w and A_s were recorded 3-5 times in order to get averaged amplitudes.
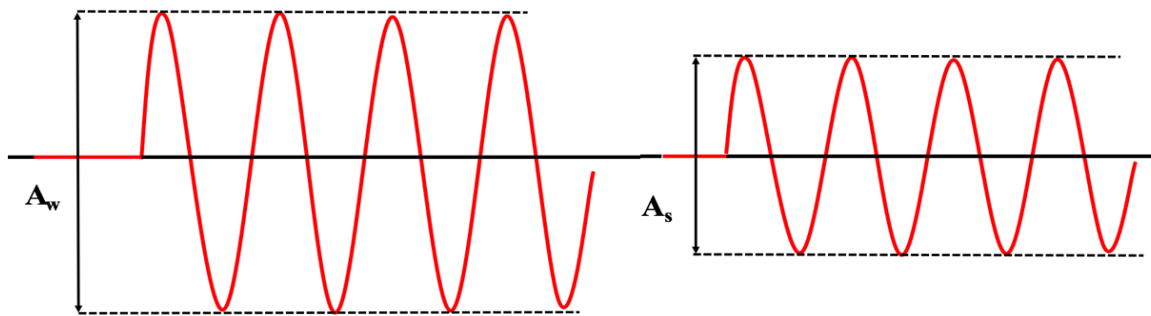
Figure 3.10: Comparison of the amplitude of the signal through the water and through the sample.

To get the equation for the attenuation coefficient, we must perform a derivation similar to the one seen in section 2.1.1. Instead of the simple scenario described by figure 2.1, in which an ideal ultrasound plane wave is incident on a specimen, experimentally an ultrasound plane wave propagates through water, through a thin layer of saran wrap, into the cell pellet, through the cell pellet and ultimately back into the water, shown in figure 3.11.
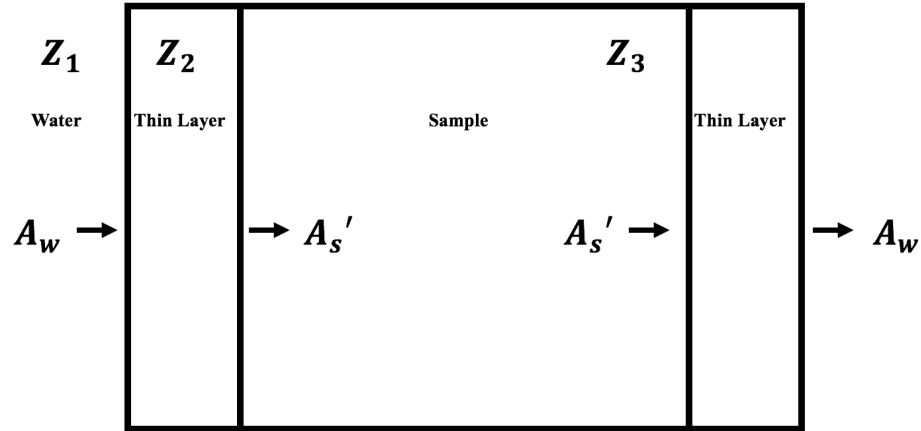
Figure 3.11: Change in the amplitude of an ultrasonic wave through as a result of the passage through three different impedances.

In figure 3.11, Z_1 is the acoustic impedance of the water, Z_2 is the acoustic impedance of the thin layer of saran wrap, and Z_3 is the acoustic impedance of the sample. For saran wrap $Z_2 = 4.25 \times 10^6 \frac{kg}{m^2 s}$. The total intensity transmission coefficient through either plastic layer is given by

$$\frac{4 Z_1 Z_3}{(Z_1 + Z_3)^2 \cos^2(k_2 l) + \left(\frac{Z_2 + Z_1 Z_3}{Z_2}\right)^2 \sin^2(k_2 l)} \tag{3.4}$$

where $k_2 l = \frac{2\pi}{\lambda_2} = \frac{2\pi f}{c_2}$. λ_2 is the wavelength, c_2 is the speed of sound in the saran wrap and f is the frequency. The thickness of the saran wrap is given by l. For saran wrap $Z_2 = 4.25 \times 10^6 \frac{kg}{m^2 s}$ and $c_2 = 2504$. The amplitude of the transmission coefficient through the plastic layer is given by $T_{ampl} = \left(\sqrt{\frac{Z_3}{Z_1}} T\right)$. The total effect of having the two layer of plastic is

$$T^2 = \left(\sqrt{\frac{Z_3}{Z_1}} T\right)\left(\sqrt{\frac{Z_1}{Z_3}} T\right). \tag{3.5}$$

After measuring the amplitude of the signal with and without the sample present, the attenuation coefficient, α in units of $\frac{dB}{cm}$ can be expressed as

$$\alpha = \frac{20}{d} \log_{10} \left(\frac{A_w T^2}{A_s} \right). \tag{3.6}$$

3.4.5 Backscatter Experimental Setup

The backscatter experiments were conducted using a pulse-echo data reduction technique described by Chen et al [28], Insana et al [29] and Madsen et al [30]. This method was designed to remove equipment-dependent effects by dividing the power spectrum of the measured data by a reference spectrum. The measured data from the reference spectrum is obtained by performing a calibration experiment where reference signals were acquired using the specular reflection from an optical flat quartz planar reflector, placed at the transducer focus.

The pulse-echo set up for the backscatter involves using one single-element focused transducer that is held in a plastic housing, shown in figure 3.12, and is fixed using two small screws. The cell pellet with the smaller diameter is held in a plastic housing connected to a thin metal rod that is controlled by the high precision stepper motor COSMOS. The scattering of ultrasound by small tissue volumes is dependent upon the orientation of the scattering elements in relation to the incident wave front, so it is important to ensure that the piezoelectric surface of the transducer is parallel to the front surface of the cell pellet, so that the distance of the transducer from the pellet is consistent while the pellet is moved in the y-z plane to perform a raster scan of nine points across the pellet, as shown in figure 3.14. To align the transducer, we physically maneuver it, via adjusting the screws that hold the transducer in the plastic housing and by adjusting the tilts of the transducer and pellet until the signal on the oscilloscope is maximized.

After alignment, we position the transducer such that the front face of the cell pellet, shown in figure 3.13 and 3.14 is located a distance away from the front surface of the transducer equal to the focal length of the transducer plus an additional offset due to the thin saran layer. Using the Virtual Jog setting on COSMOS, along motor 1 (the x-axis), the cell pellet is moved towards or away from the transducer, until it is the appropriate distance away. This distance is calculated as a time delay, given by the equations

$$2d = \left(\text{offset} + \frac{\text{window}}{2}\right) C_s, \tag{3.7}$$

$$\delta = f - d, \tag{3.8}$$

and

$$t_d = \frac{2\delta}{C_w} \tag{3.9}$$

where 2d represents the distance of the signal traveling through the cell pellet and back, the offset is the time in the sample before we start sampling (1.5 μs), window refers to the "window" of time used to gather the RF data (10 μs), C_s is the sound speed of the sample (determined by the attenuation experiment), δ is the distance of the signal traveling to the sample, f is the focal length of the sample, C_w is the speed of sound through water, and t_d is the time delay (the distance we want to put the transducer away from the cell pellet).

Using motor 1 and by looking at the signal on the oscilloscope, we can identify the front face and the back face of the cell pellet. On the oscilloscope, the signal appears as an envelope which shows the variations in amplitude of the waveform produced by the scattered signal against a time scale. The first high amplitude signal seen on the oscilloscope corresponds to the interface where the front face of the cell pellet meets the surrounding water (the front face of the cell pellet is the thin saran layer). The set of signals that follows is recognized as the cell

scatterers that are distributed in the agarose pellet and the amplitude of these signals is smaller than that of the signal through the saran layer. Next, there is another set of high amplitude signals corresponding to the back face of the cell pellet (which is another saran layer), that appear very similar to the first high amplitude signal seen, due to the front face of the sample.

Once the front face of the cell pellet is identified, the time delay on the oscilloscope is set to the correct amount as per the calculations done in equations 3.7-3.9.
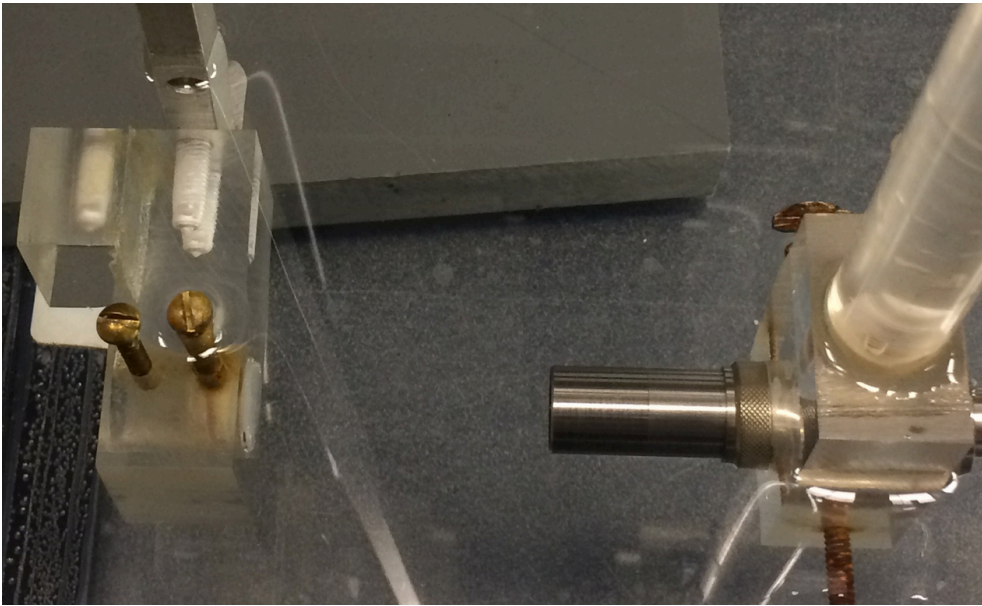
Figure 3.12: Laboratory setup for backscatter coefficient experiment.
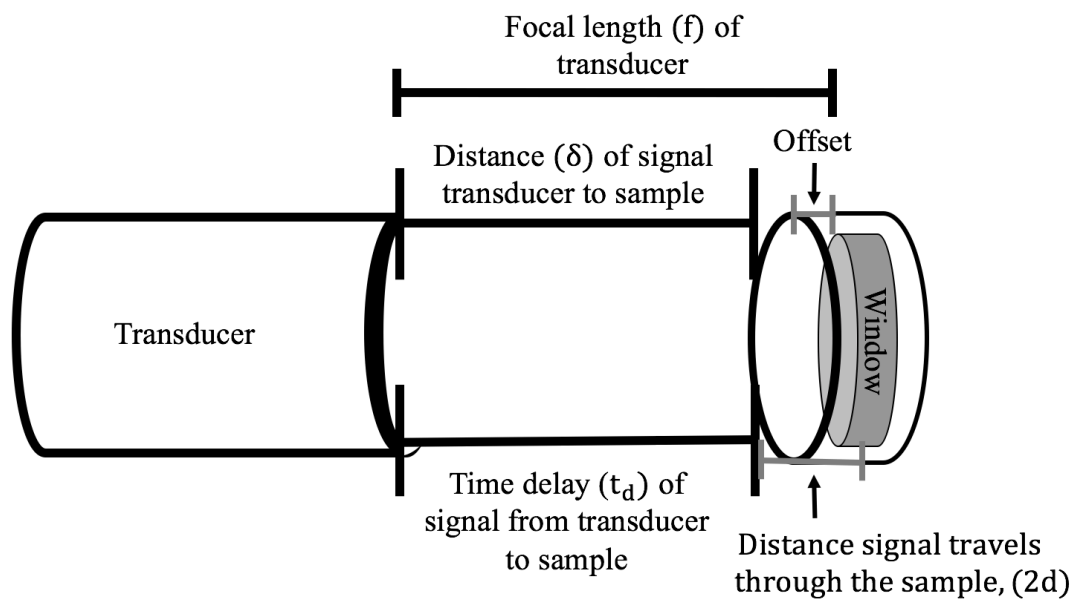
Figure 3.13: Determination of the correct distance the transducer must be placed away from the cell pellet.

The focal length of the transducer beam is due to the nature of each individual transducer and can be obtained from the data sheets sent from the manufacturer. Table 3.1 shows the focal length of each transducer.

Table 3.1: Summary of focal lengths for transducers at different frequencies

Transducer (MHz)	Focal Length (mm)
5	52.172
10	51.664
15	51.841
20	30.53
25	31.369

Once the cell pellet and transducer are positioned at the correct distance, we need to position the cell pellet so that the very center of the pellet is in line with the transducer's signal.

In order to center the pellet, the edges of the cell pellet holder must be found, using COSMOS Quick Move motor 2 (y-axis) and motor 3 (z-axis), as portrayed in figures 3.7 and 3.14, and by looking at the waveform on the oscilloscope. In a similar manner to how we identified the front and back face of the cell pellet, we can identify edges, 1, 2, 3, 4 of the cell pellet, by observing the change in amplitude in the signal on the oscilloscope. On the edges the amplitude of the signal increases significantly and looks like a spike.

Using the Quick Move mode motor 3 and setting the step size to 250, we begin to move cell pellet along the z-axis, towards edge 1. A step size of 250 is small enough that we will not overshoot the edge and can achieve a quality alignment. Once at edge 1, we move the cell pellet towards edge 2, still along the z-axis and keep track of how many steps it takes. Once the signal hits edge 2, we stop movement and divide the number of steps it took to traverse from edge 1 to 2 in half. This is the distance to the center of the sample in the z direction. We then move the transducer back the determined number of steps and repeat this process using motor 2 (along the y-axis). The transducer is now centered over the cell pellet, and correctly aligned in all directions. By ensuring correct alignment, our data will be consistent across samples.
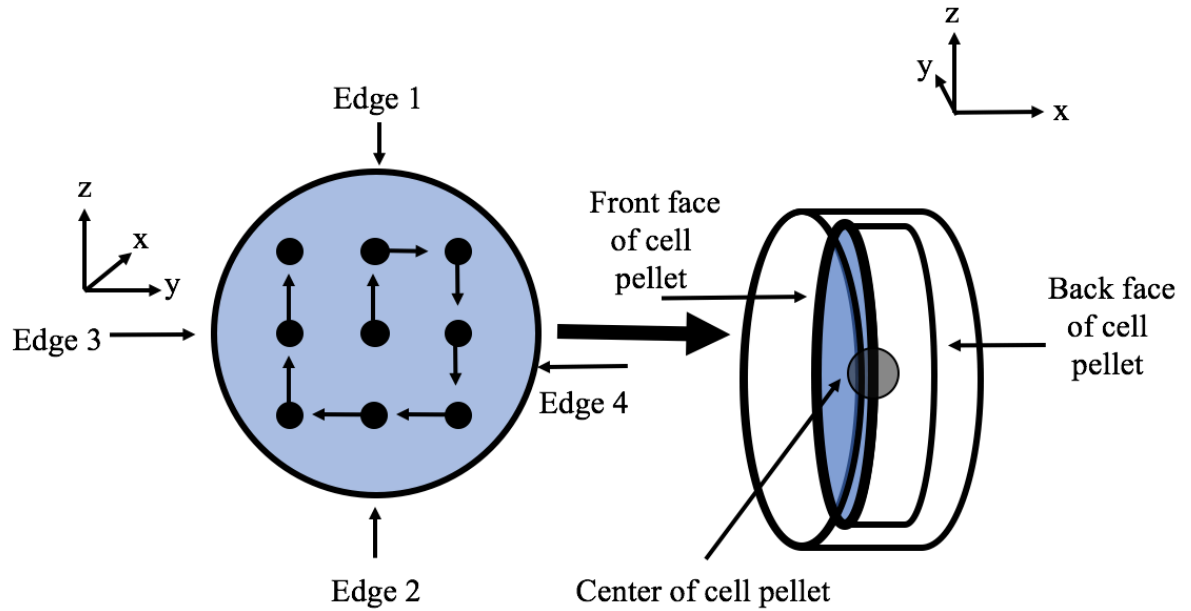
Figure 3.14: Nine-point spiral setup for raster scan over the cell pellet with a diagram of the edges, front face and back face of the cell pellet.

3.4.6 Backscatter RF Data Collection

After correct alignment, the objective of the backscatter experiment is to collect RF pulse-echo signals and using MATLAB [31] to convert the signal information into backscatter coefficients. To reduce noise multiple scans of the same sample are taken. We collect RF pulse-echo data at nine points by taking a raster scan across the cell pellet. We only collect data at nine points due to the size of the cell pellet. Figure 3.14 includes a schematic diagram of the raster scan that shows the spiral pattern used to collect data at the nine points, starting at the center of the pellet, hence the importance of centering the transducer initially. Using the Quick Move mode on COSMOS and motors 2 (y-axis) and 3 (z-axis) with a step size of 331 we can complete this scan pattern.

The diameter of the black circles in the nine-point spiral setup in figure 3.14 represent the diameter of the transducer's beam when it hits the sample face. The step size represents the distance we need to go to not have overlapping points when we gather data at each of the nine points. We get appropriate step sizes by assuming our focus is diffraction limited and using the equation

$$w = \frac{1.22f\lambda}{2r} \tag{3.10}$$

where w is the width of the transducer beam, f is the focal length of the transducer, λ is the frequency of the transducer, and r is the radius of the transducer. Figure 3.15 shows the schematic of the geometry for a transducer beam width and using Snell's Law we can equate the angle of incidence to the frequency of the transducer in use. Additionally, using the law of sines and assuming that θ is small, we can do the conversion, $\tan \theta = \frac{w}{f} \rightarrow \theta = \frac{w}{f} \rightarrow \frac{w}{f} = \frac{1.22\lambda}{2r}$. After finding the beam width, we double it to prevent overlapping and then convert it to "steps" to get the appropriate step size.
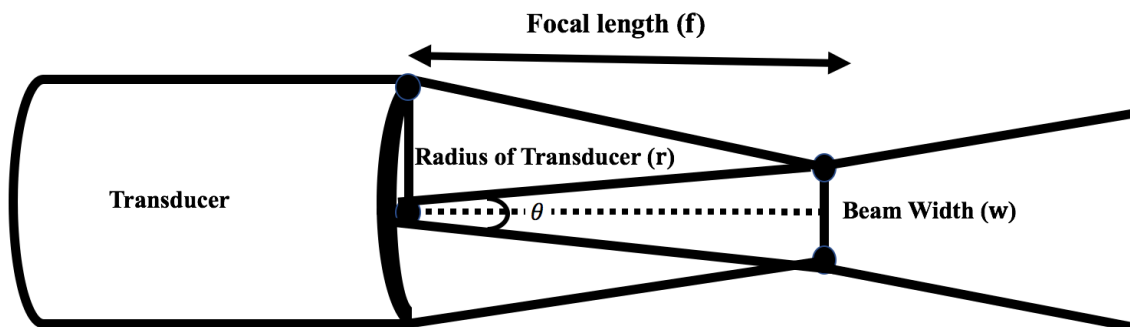
Figure 3.15: Schematic of the geometry to determine a transducer's beam width

To collect the RF data, we take the steps one at a time letting the signal settle before moving onto the next step. The movement of the pellet disturbs the water and this distortion can

disrupt or distort the signal. Once the signal is settled, we save the RF voltage trace data from the oscilloscope to an external USB drive. This procedure is repeated for each of the nine data points. After collecting all the data, it is processed in MATLAB [31].

3.4.7 Calibration Experimental Setup

The pulse-echo set up for the calibration of the equipment is very similar to that of the backscatter, demonstrated in figure 3.15. To get the RF echoes particular to each individual single-element focused transducer, we secure the transducers (one at a time) in a plastic housing, and hold them in place using two small screws. The quartz planar reflector is held in a plastic housing that is controlled by the high precision stepper motor COSMOS. We use the quartz planar reflector for the calibration due to its high reflecting properties. To align the transducer so that it's piezoelectric surface is parallel to the planar reflector, we first physically adjust the transducer so that visually the signal appears to be propagating through the center of the planar reflector. To further ensure that the front surface of the transducer is parallel to the reflector, we must check for tilt in the reflector. Ideally the reflector is positioned so that is perfectly parallel along the z-axis given by figure 3.7, meaning there is no tilt to the reflector. To ensure this is true, we move the reflector using the Virtual Jog mode on COSMOS in the x and z directions, and observing the waveform on the oscilloscope as the reflector moves. The amplitude of the waveform should not change, nor should the resultant signal move in time. If it does either, we know that the reflector is tilted in the along the x-axis (tilted towards or away from the transducer). We then adjust the tilt, by using the knob on the plastic housing holding the planar reflector, shown in figure 3.15, until the waveform no longer moves in time. It is important to note that due to the uniformity of the planar reflector, distance between the transducer and the

reflector is less important, and we only the information of the resultant signal at one data point is needed, instead of nine.
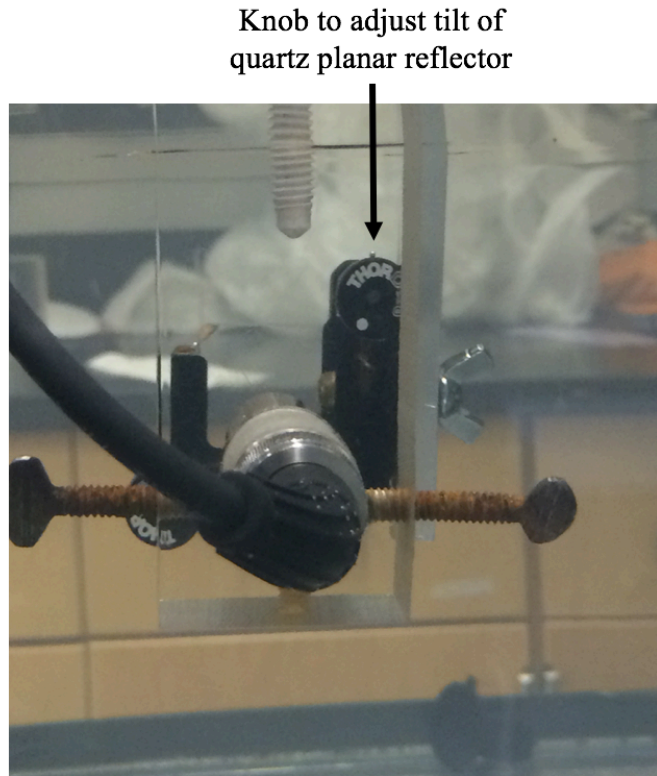
Figure 3.16: Laboratory setup for calibration of equipment.

3.4.8 Flat Quartz Planar Reflector RF Data Collection

To collect the data from the flat quartz planar reflector, we follow the same procedure as the backscatter RF data collection, but instead of saving nine RF signals to the USB drive, we only need to save one. In addition to saving the RF data to the USB drive, we also record the pulse width of the signal. This measurement is difficult to do accurately because the strong reflectivity of the planar reflector results in many echo pulses seen on the oscilloscope which are

hard to distinguish from the first reflected pulse. In determining the beam width, one might accidentally include the length of an echo pulse as well.

3.4.9 Backscatter and Calibration Processing

The collected data is processed using programs on MATLAB [31]. The RF voltage trace data is saved as .cvs files, which are fed into a program that produces a list of the planar spectra values (a Fourier transform of the RF data collected using the planar reflector), the sample spectra values (a Fourier transform of the RF data collected using the cell pellet), the frequencies used, and the backscatter coefficients. We take all of the outputted data and transfer it to an excel spread sheet where we can make graphs of the planar spectra v. frequency, sample spectra v. frequency and backscatter v. frequency.

3.4.10 Backscatter and Calibration Electronic Setup

For data collection, we used an Olympus Parametric-NDT wide band 5678 preamplifier Olympus Parametric-NDT 5073PR pulser/receiver, and a Tektronix TDS 3014C digital phosphor oscilloscope with 1.25 GS/s digitalization. The pulser/receiver served to send out a short voltage pulse, which is then turned into an ultrasonic pulse by the transducer. The same transducer then receives the returning wave at its piezoelectric element and the preamplifier amplifies the signal before it is displayed on the oscilloscope.

The transducer is attached to the mounting bracket of a male UHF adaptor on a BNC cable. A female BNC T adaptor is connected to the other end of the cable and two more cables are hooked to the female adaptor. One cable is fed into the preamp and the other is fed into the trigger/receive point on the pulser/receiver. The output of the preamp is connected to the receive port on the pulser/receiver. The sync out of the pulser/receiver was linked with the external

trigger of the Digital Phosphor Oscilloscope and the sig out of the pulser/receiver was connected to Channel 1 of the oscilloscope. This electronic setup is shown in figure 3.16.

The gain on the pulser/receiver and the voltage of the window on the oscilloscope differed for different transducers. For the duration of experiments the PRF was set to 500, energy was set to 3, damping was set to 3, and the low pass frequency (LPF) was set to 5MHz. The high pass frequency (HPF) was set to 20 MHz when using the 5, 10, and 15MHz transducers, and set to the full bandwidth for the 20 and 25MHz transducers. It is important to record the settings on the pulser/receiver for each backscatter experiment because they have to be exactly the same during the calibration experiment in order to get an accurate description of the properties of the electronics.
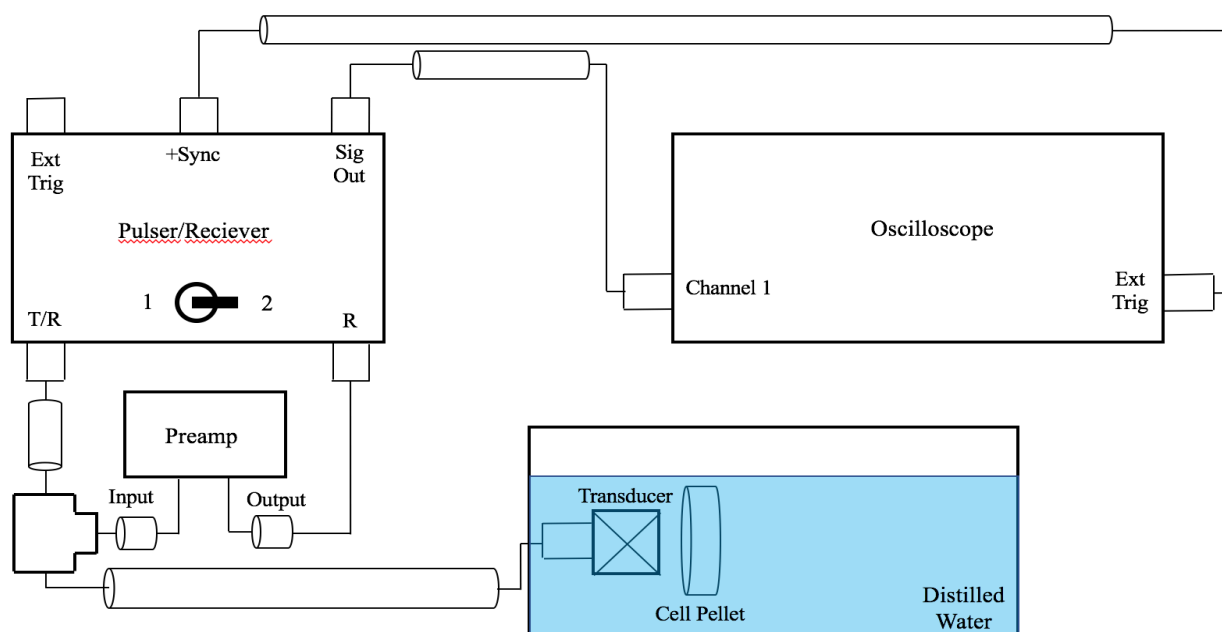
Figure 3.17: Electronic setup for the backscatter and calibration experiments

3.4.11 Backscatter Coefficient Experimental Calculation

To get the backscatter coefficient experimentally, we use the equation derived by Chen *et al*. [28], Madsen *et al*. [30] and Insana [29].

$$\eta(\omega) \approx \frac{\langle V_g(\omega)V_g^*(\omega)\rangle}{C^2|T(\omega)B(\omega)|^2 \int\int_\Omega\int|A(\vec{r},\omega)|^4 d\vec{r}} \tag{3.11}$$

where $\eta(\omega)$ is the backscatter coefficient, the numerator, $\langle V_g(\omega)V_g^*(\omega)\rangle$, is the power spectrum of the sample, and the denominator calibrates for system properties including the speed of sound, C^2, properties of the electronics, $T(\omega)B(\omega)$, and the beam profile (the shape and size of the piezoelectric element, and the attenuation of the signal) integrated over 3 dimensions, $\int\int_\Omega\int|A(\vec{r},\omega)|^4 d\vec{r}$.

$V_g(\omega)$ represents discrete Fourier transforms of RF voltage trace data for each of the nine data points. The mean value of the square moduli of the Fourier transform yields, $\langle V_g(\omega)V_g^*(\omega)\rangle$ which is the power spectra of the sample reflector signal [25]. $T(\omega)B(\omega)$ accounts for the system frequency response, where $T(\omega)$ is the frequency-dependent complex receiving transfer function of the transducer that depends on the total force averaged over the transducer surface and the voltage generated by the transducer and $B(\omega)$ is a complex superposition coefficient that determines the frequency content of the incident pulse [30]. $T(\omega)B(\omega)$ is given by the equation

$$T(\omega)B(\omega) = \frac{\widetilde{V}_r(\omega)}{R\int\int_{Smirror}A_0(\mathbf{r},\omega)ds} \tag{3.12}$$

where $\widetilde{V}_r(\omega)$ is the Fourier transform of the echo signal voltage due to the presence of the planar reflector (the power spectra of the planar field), R is the ampltitude reflection coefficient for the planar reflecting surface, $A_0(\mathbf{r},\omega)$ is the transducer field beam profile integrated over two dimensions (because it is reflecting off the surface). $A_0(\mathbf{r},\omega)$ is computed using the diameter and focal properties of the transducer.

Chapter 4

Results

4.1 HCT Cell Concentration

A total of eight HCT of different viable cell concentrations were used for

experimentation. The viable cell concentration is calculated by multiplying the mean number of

viable cells with a dilution and a correction factor (given by equation 3.1) and is presented in

table 4.1.

Table 4.1: Summary of viable cell concentrations of the HCT cell pellets

	Backscatter Concentration of viable cells (cells/mL)	Attenuation/Speed of sound Concentration of viable cells (cells/mL)
Experiment 1:	2375×10^4	2209.5×10^4
Experiment 2:	1337.5×10^4	2205×10^4
Experiment 3:	2205×10^4	1327.5×10^4
Experiment 4:	234×10^4	274.5×10^4

4.2 HCT Cell Pellet Speed of Sound

Table 4.2 shows the average speed of sound of the cell pellets at different frequencies.

We used equation 3.3 to calculate the speed of sound through the pellet.

Table 4.2: Summary of the average sound speed of the HCT cell pellets

Transducer frequency (MHz)	Average speed of sound of sample (m/s)
5	1521

10	1521
15	1521
20	1523
25	1523

4.3 HCT Cell Pellet Attenuation

Figure 4.1 presents the mean attenuation coefficients of the HCT cell pellets averaged over four sets of measured data, plotted as a function of frequency between 5-30 MHz and the polynomial least squares straight line was fitted to the data set. The polynomial least squares straight line is given by

$$Y = ax^2 + bx + c \rightarrow Y = 0.0038x^2 + 0.0372x - 0.0323 \qquad (4.1)$$
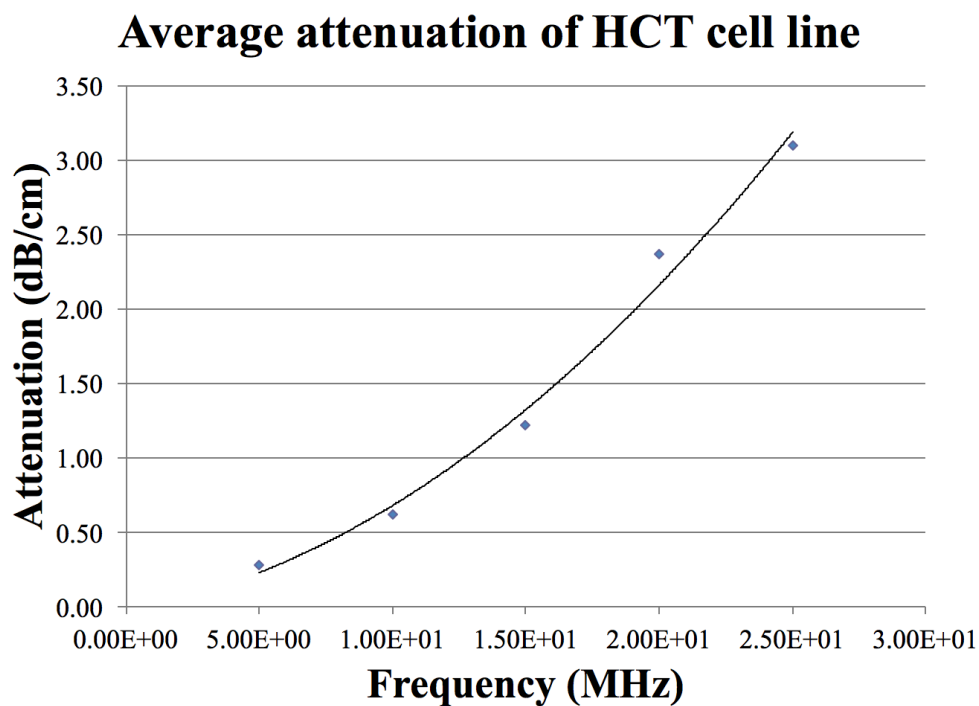
Figure 4.1: Estimated attenuation coefficient versus frequency with polynomial least squares best fit straight line for all cell pellets. Estimated attenuation of each cell pellet is based on data

acquired from five single element focused transducers: 5 MHz, 10 MHz, 15 MHz, 20 MHz and 25 MHz. There are four cell pellets for each measurement.

4.4 HCT Cell Pellet Backscatter

The BSC estimates of the HCT cell pellets are shown in figure 4.2 The BSC versus frequency curves for different frequencies shares a similar pattern in the sense that there is a "ringing" behavior seen in all of the curves where the backscatters coefficients seem to be oscillating. Additionally, the BSC changes with frequency. For the BSC at 5 MHz, 10 MHz and 15 MHz, as the frequency increases so does the BSC. There is an offset at the 20 MHz and 25 MHz and they have lower BSC values than the 5, 10 and 15 MHz BSC values. However, from their starting point we see an increase in the BSC as the frequency increases.
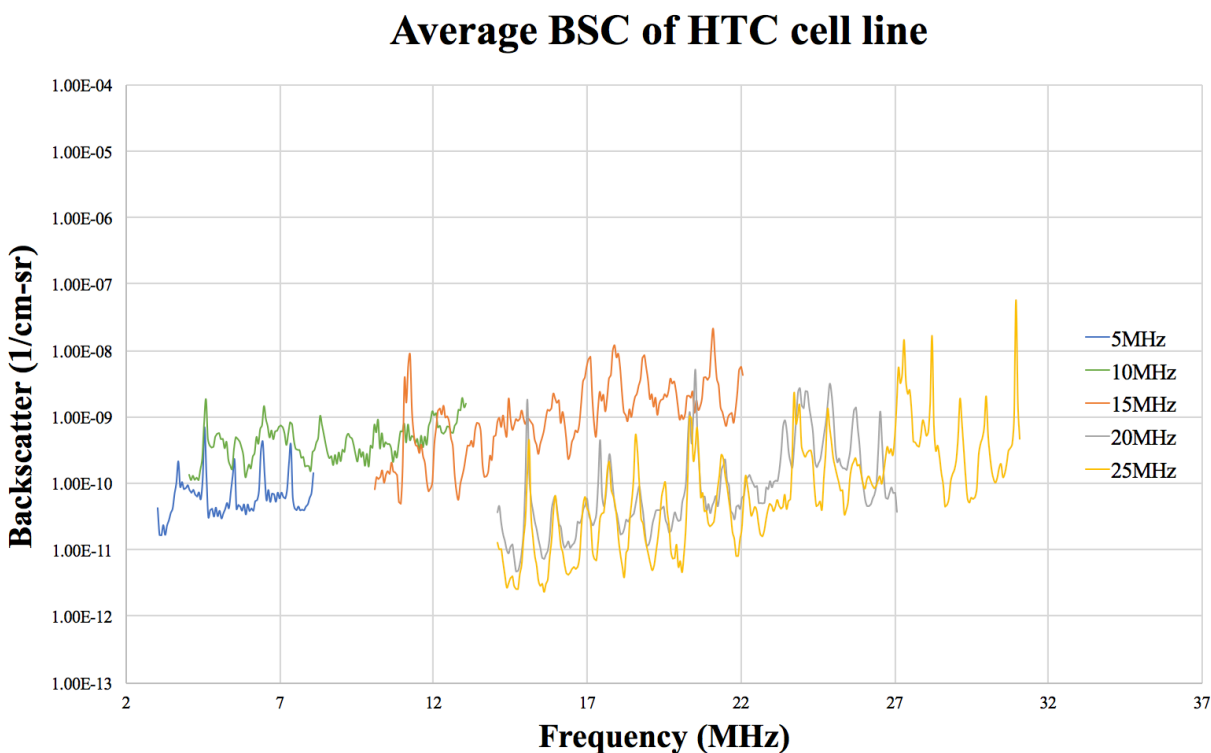
Figure 4.2: Estimated BSC vs. frequency for all HCT cell pellets. Estimated BSC of each cell pellet is based on data acquired from five single element focused transducers: 5 MHz, 10 MHz, 15 MHz, 20 MHz and 25 MHz. There are four cell pellets for each measurement.

4.5 Comparison of the Sample Spectrum, Planar Reflector Spectrum and the Transducer Spectrum

Figures 4.3-4.7 illustrate the spectra for the sample (a), the planar reflector (c) and the for the transducer (b). The transducer spectrum comes from the data provided by the manufacturer for each of the single-element focused transducers that were used for the backscatter measurements. There is expected to be some noise the sample spectra because it is an inhomogeneous medium, but the ringing behavior seen in the planar spectrum is unexpected.
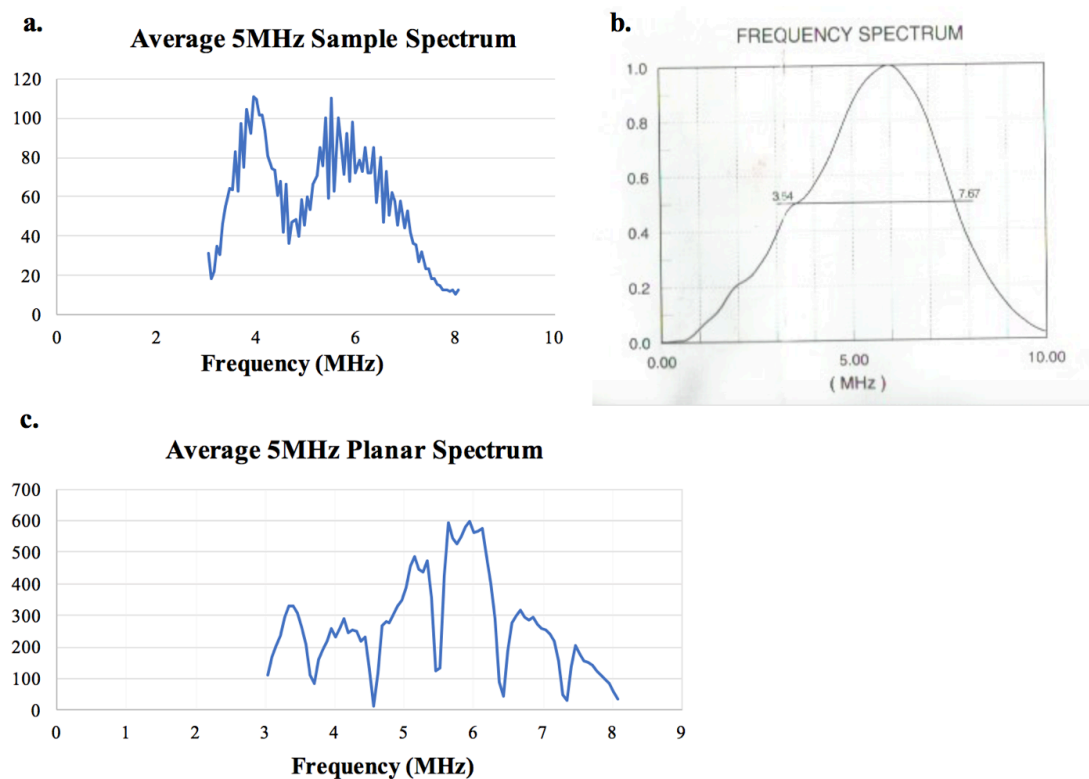
Figure 4.3: Comparison of the spectrum for the HCT cell pellet (a), the flat optical quartz planar reflector (c), and the manufacturer's data for the spectra of a 5 MHz single element ultrasound transducer (b).
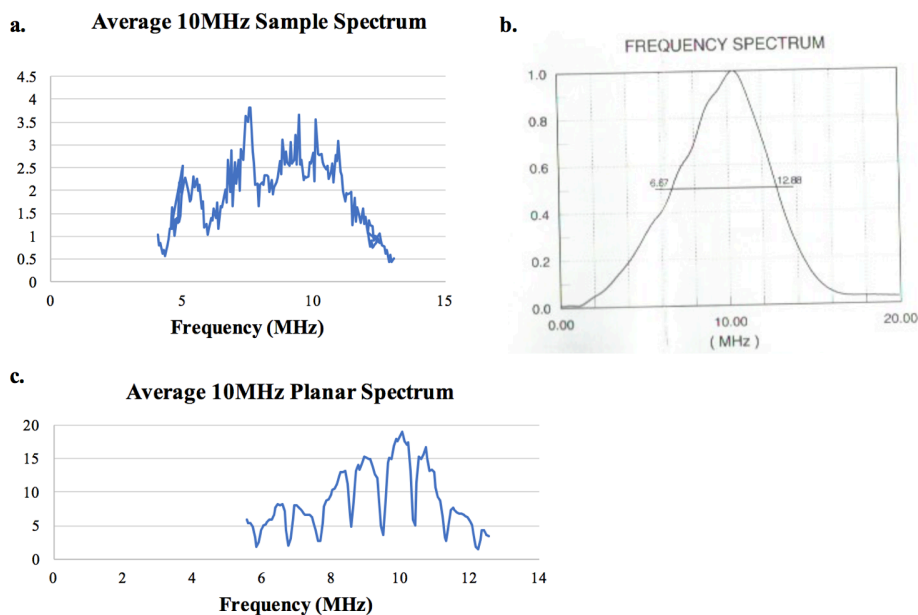
Figure 4.4: Comparison of the spectrum for the HCT cell pellet (a), the flat optical quartz planar reflector (c), and the manufacturer's data for the spectra of a 10 MHz single element ultrasound transducer (b).
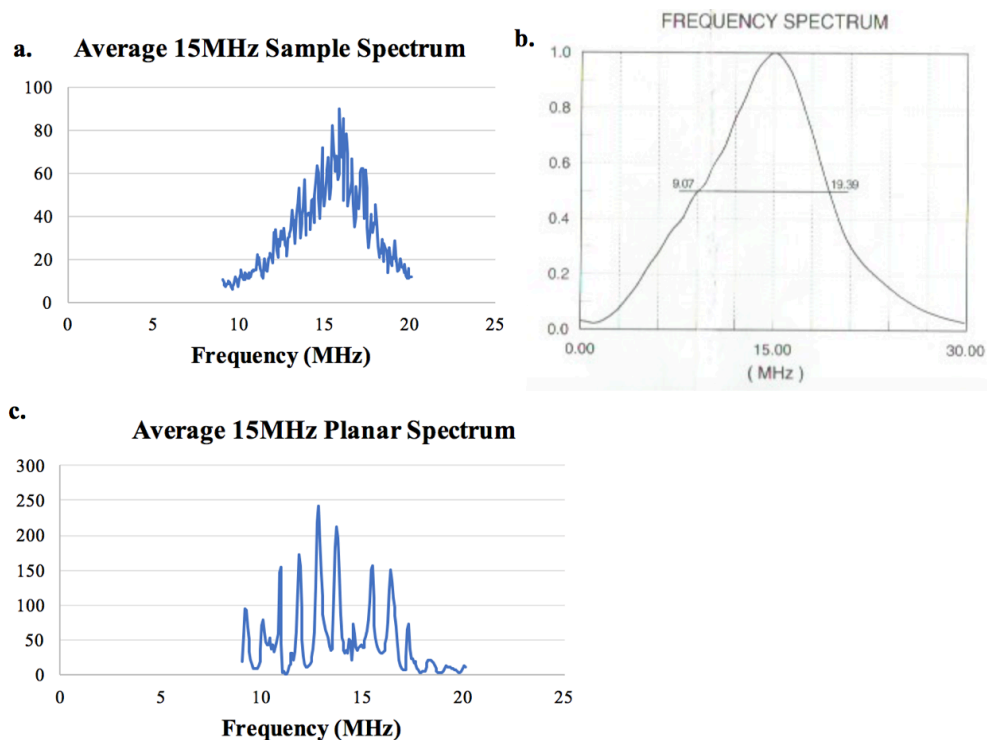
Figure 4.5: Comparison of the spectrum for the HCT cell pellet (a), the flat optical quartz planar reflector (c), and the manufacturer's data for the spectra of a 15 MHz single element ultrasound transducer (b).
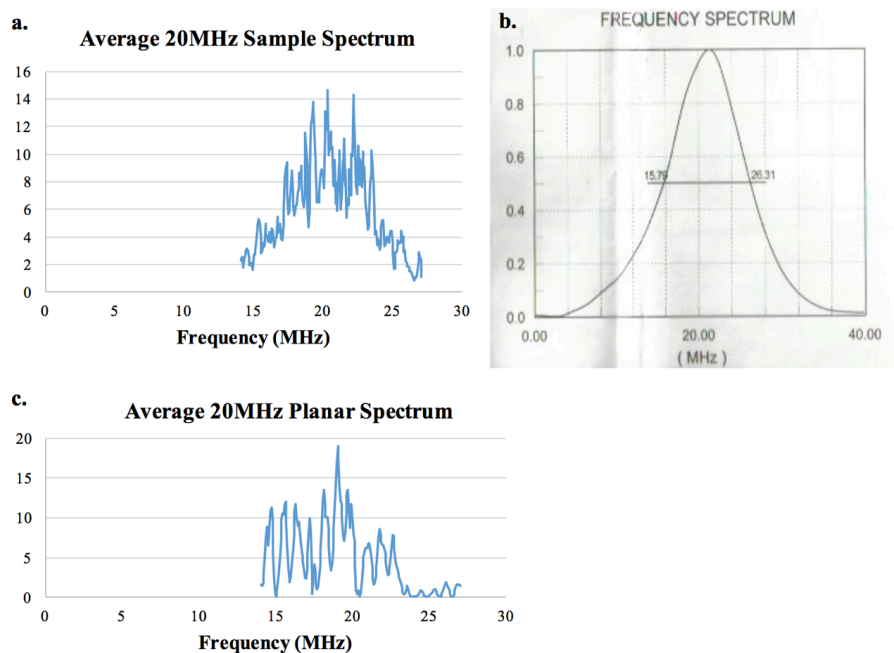
Figure 4.6: Comparison of the spectrum for the HCT cell pellet (a), the flat optical quartz planar reflector (c), and the manufacturer's data for the spectra of a 20 MHz single element ultrasound transducer (b).
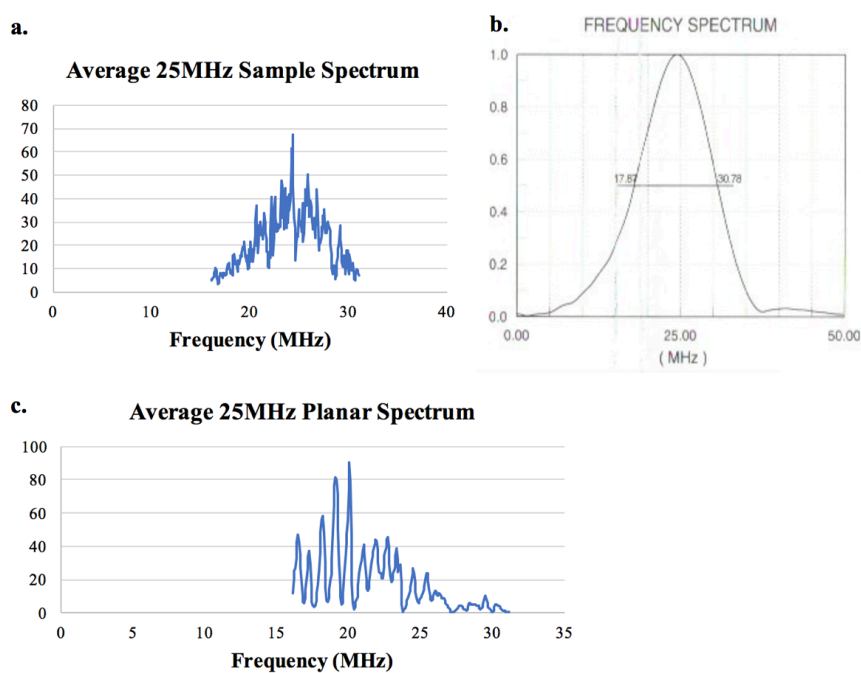
Figure 4.7: Comparison of the spectrum for the HCT cell pellet (a), the flat optical quartz planar reflector (c), and the manufacturer's data for the spectra of a 25 MHz single element ultrasound transducer (b).

Chapter 5
Analysis and Discussion

Previous experimentation conducted by other researchers in have shown that this method of using the cell pellet biophantom and similar ultrasonic techniques to get quantitative information about the scattering of the cells is valid [14,15, 32]. However, no previous work has been done using the HCT cell line, so no comparisons can be made with this and other works. It is for this reason that we have no strong expectations for what our backscatter and attenuation curves should look like.

### 5.1 HCT Viable Cell Concentration Analysis

As stated in section 3.1.1 we grew the HCT cells on a culture flask for a week before using them to make a cell pellet, so that we would have roughly the same concentration of viable cells for every experiment. However, as seen in Table 4.1 the concentration of the viable cells is varied. The counting of the cells was performed by mixing $150\mu L$ of cell solution with $150\mu L$ of Trypan blue and using a hemocytometer to count the dead cells (section 3.1.2). This process was difficult to do because this strain of cells was very clumpy, meaning they did not like separate when vortexed or mixed. Often additional gentle pipetting was needed in order to disperse the cells as evenly as possible. Due to this feature, sometimes when we pipetted $150\mu L$ of the cell solution we would get a large cluster of the cells which we would then pipet back into the cell solution so that more cells would be in the cell pellet rather than used for counting. Other times when we pipetted $150\mu L$ of the cell solution we would extract only a few cells with which to perform the cell count. It is for these reasons that we are believe our viable cell concentrations are implausible.

5.2 HCT Cell Pellet Speed of Sound Analysis

We see good agreement of the speed of sound through the cell pellet across the frequencies. As expected the speed of sound is faster through the cell pellet than the water (water at 33° C has a sound speed of ≈ 1516 m/s).

5.3 HCT Cell Pellet Attenuation Analysis

As stated previously, we have there does not exist any previous attenuation for HCT with which to compare our results to. However, comparing our results to prior studies measuring the attenuation and backscatter of CHO (Chinese Hamster Ovarian) cells [14, 15], we can see that the attenuation does behave in a manner that we expect: as the frequencies increase the attenuation increases as a power function (figure 4.1). This behavior agrees with the theoretical equations 2.7 and 2.8 we derived in section 2.1.1 as well as the experimental equation 3.6 we derived in section 3.4.4. Overall, we can safely say that our attenuation results look consistent with previous studies.

5.4 HCT Cell Pellet Backscatter Analysis

Although we do not have any previously existing BSC measurements to compare our experimental BSC to, looking at the BSC of different cell lines [14, 15, 32, 33, 34] we can get an idea of what the curves theoretically should look like. Unfortunately, our BSC curves do not look as expected. The ringing behavior is very unusual as well as the offset of the 20 MHz and 25 MHz (figure 4.2). By looking at figures 4.3-4.7, the sample spectrum and planar spectrum (Fourier transforms of the cell pellet RF data and planar reflector RF data), and comparing it to the manufacturer provided curve, we think the ringing behavior is coming from the RF data of the planar reflector. In figures 4.3-4.7 we see that the shape of the curves of the spectra for the

HCT cell pellets generally match the shape of the curve for the transducer given by the manufacturer at different frequencies. We do not expect the cell pellet spectra curve to exactly match that of the transducer because the cell pellet is an inhomogeneous medium and some frequency response due to the cells is expected. The shape of the spectra for the flat optical quartz planar reflector does not match the curve of the transducer given by the manufacturer. Instead it seems to have a ringing behavior. We think the error in the planar spectra could be reduced by increasing the number of independent line of RF echo data used to estimate the power spectra and by repeating the measurements (instead of being measured just once). Also, we are considering how the MATLAB program interprets the RF echo signal from the planar reflector and making some adjustments to the program so that the signal can be processed appropriately.

Chapter 6

Conclusion and Future Work

Through our experimentation, we have found that we can successfully use quantitative ultrasound techniques to characterize HCT cell pellets. Using unfocused transducers in the 5-25 MHz range we were able to make satisfactory measurements of the attenuation and speed of sound. Using focused transducers in 5-25 MHz range we saw some variance in the backscatter coefficient estimates which we attribute to poor power spectral density estimates for the echo signals from the planar reflector.

There is much work to be continued. First, new RF echo signals using the quartz optical planar reflector must be measured. Additionally, we need to check the MATLAB programs to see if they are processing the RF signals from the planar reflector correctly. The attenuation, speed of sound, and backscatter experiments and measurements should be repeated in other labs to check for consistency in the estimates. We can continue our measurements at higher frequencies to see the scattering behavior at subcellular levels and we can start measurements for benign colon cells to explore if there is a difference in the ultrasonic characteristics of malignant and benign cell lines.

Appendix A

Table of the Electronic Settings Used in the Backscatter Experiment

Frequency (MHz)	Gain (dB)	Voltage (mV)
5	-9	50.0
10	35	5.00
10	-04	20.0
15	05	50.0
20	05	20.0
25	05	50.0

Here the 10 MHz is listed twice because for one of our measurements we did not use the preamplifier so the pulser/receiver had different settings.

Appendix B

Table of the Electronic Settings Used in the Calibration Experiment

Frequency (MHz)	Gain (dB)	Voltage (mV)
5	-25	50.0
10	-20	5.00
10	-25	20.0
15	-36	50.0
20	-43	20.0
25	-36	50.0

For the calibration experiment we want to take pulse echo RF data of the planar reflector at the same voltage as we did for the backscatter, so we adjust the gain.

Appendix C

MATLAB Program to Calculate the Backscatter Coefficient
(The parameters in this code are for the 5 MHz transducer)

```
%Input parameters for 5MHz:
a = 6.35; %'Enter projected radius of transducer (mm)
Cw = 1515.78;  %'Enter sound speed of water (m/s):
quartzReflect = .796; %reflection coeffieicnt for planer relfector
alpha0 = -.0323;
alpha1 = .0327 ; %('Enter alpha1 [attenuation = (alpha1)x +
(alpha2)x^2]: ');
alpha2 = .0038; %('Enter alpha2 [attenuation = (alpha1)x +
(alpha2)x^2]: ');
Cs = 1521; %('Enter sound speed of sample (m/s): ');
rcurv = 26.086; %('Enter transducer''s radius of curvature(mm): ');
tsd = 4.7232; %('Enter transducer-sample surface distance (cm): ');
z0 = 4.837275; %('Enter beginning axial distance of sampled volume
(cm): ');
FilePath = 'C:
\Users\mhcuser\Desktop\Amy'sBackscatter\Backscatter323\5MHz'; % path
to data files
FileNameBase = '10Mfebll_'; %filename base
PlanerPath = 'C:\Users\mhcuser\Desktop\Backscatter\Calibration\PR10';
% path to planer reflector files
PlanerName = 'TEK00009.CSV'; %planer reflector filename.
currfftlength1024 = 16484; %needs to be at least as long as the length
of data
winsize = 10;  % window size in microseconds
numFrame = 8; %number of raster scan points
fLow = 1;    % in MHz
fHigh = 8;   % in MHz

%%%%%%%%%%%%%%%%%%%%%%%%%%%%%%%%%%%%%%%%%%%
%Unit conversions of inputs:
a = a * (1E-3); %in meters
fLow = fLow*1000000; %(Hz)frequency in hz
fHigh = fHigh *1000000; %(Hz)frequency in hz
rcurv = rcurv * .001; %(m)radius of curvature in m
tsd = tsd*.01; %transducer sample distance in (m)
z0=z0*.01;



%load the data
%sampleData = [];

k=char(49);
l=1;
 FileName = strcat(FileNameBase,k,'.csv');
 firstdata =[];
 firstdata = loadRFdata(FilePath, FileName);
 amountdata = double(length(firstdata));
  %size(firstdata)
 sampleData = zeros(amountdata,2,numFrame);% 'int32');
```

```
 %size(sampleData)
 %size(sampleData(:,:,l))
sampleData(:,:,l) = sampleData(:,:,l) + firstdata(:,:);

for i = 2:numFrame
 j = char(48+i); %note this will not work for files greater than 9 –
need a better option.
 FileName = strcat(FileNameBase,j,'.csv');
 sampleData(:,:,i) = sampleData(:,:,i)+ loadRFdata(FilePath,
FileName);
end
%size(sampleData)
% sampleData
planerData = zeros(amountdata,2,'int32');
planerData = loadRFdata(PlanerPath, PlanerName);
%get power spectra of data – this also corrects attenuation
SampleSpectra = powerSpectra(sampleData, winsize, currfftlength1024,
fLow, fHigh, numFrame,alpha0, alpha1, alpha2, rcurv, tsd);

%pressure focusing gain of transducer
winsizeDP = length(sampleData);      % Window size in DFT sample points
currSamRate = winsizeDP/(winsize*.000001);
st_freq = round(fLow*currfftlength1024/currSamRate) + 1;  %
10/14/2006, Convert frequency to DFT sample index
end_freq = round(fHigh*currfftlength1024/currSamRate) + 1;  %
10/14/2006, Convert frequency to DFT sample index
freqlength = end_freq – st_freq + 1;
 totalPFGT = zeros(1,freqlength);
 size(totalPFGT)
 freqlist = []; % in MHz
 for i = 1:freqlength;
    freqat = (st_freq –1 +i)*currSamRate/currfftlength1024;
    freqlist(i) = freqat;
   pfgt = a^2*pi*freqat/(rcurv*Cs);
     totalPFGT(1,i) =totalPFGT(1,i)+ pfgt;
 end
freqlist=shiftdim(freqlist,1)/1000000;

 %plot power spectra
 figure, plot( freqlist, SampleSpectra); grid on;



%get power spectra of planer reflector
PlanerSpectra = powerSpectraPlaner(planerData, winsize,
currfftlength1024, fLow, fHigh);
 figure, plot( freqlist, PlanerSpectra); grid on;

%    size(SampleSpectra)
%   size(PlanerSpectra)
```

```
%  size(totalPFGT)
 totalPFGT = shiftdim(totalPFGT,1);

%calculate backscatter coefficient
powerSpectraTerm = SampleSpectra./PlanerSpectra;
areaTransducer = pi*a^2;
moreConstants =2.17*rcurv^2*quartzReflect^2/(winsize*Cs/2);
% size(powerSpectraTerm)
%finalcombo
BSC = moreConstants*areaTransducer*totalPFGT.*powerSpectraTerm;
scaleGraph = double(length(BSC))
 figure, plot(freqlist(1:scaleGraph), BSC(1:scaleGraph)); grid on;
```

```
%%%%%%%%%%%%%%%%%%%%%%%%%%%%%%%%%%%%%%%%%%
%Unit conversions of inputs:
a = a * (1E-3); %in meters
fLow = fLow*1000000; %(Hz)frequency in hz
fHigh = fHigh *1000000; %(Hz)frequency in hz
rcurv = rcurv * .001; %(m)radius of curvature in m
tsd = tsd*.01; %transducer sample distance in (m)
z0=z0*.01;
```

```
%load the data
%sampleData = [];

k=char(49);
l=1;
 FileName = strcat(FileNameBase,k,'.csv');
 firstdata = [];
 firstdata = loadRFdata(FilePath, FileName);
 amountdata = double(length(firstdata));
%  size(firstdata)
 sampleData = zeros(amountdata,2,numFrame);% 'int32');
%  size(sampleData)
%  size(sampleData(:,:,l))
 sampleData(:,:,l) = sampleData(:,:,l) + firstdata(:,:);

for i = 2:numFrame
 j = char(48+i); %note this will not work for files greater than 9 –
need a better option.
 FileName = strcat(FileNameBase,j,'.csv');
 sampleData(:,:,i) = sampleData(:,:,i)+ loadRFdata(FilePath,
FileName);
end
%size(sampleData)
% sampleData
planerData = zeros(amountdata,2,'int32');
planerData = loadRFdata(PlanerPath, PlanerName);
%get power spectra of data – this also corrects attenuation
SampleSpectra = powerSpectra(sampleData, winsize, currfftlength1024,
fLow, fHigh, numFrame,alpha0, alpha1, alpha2, rcurv, tsd);
%get power spectra of planer reflector
PlanerSpectra = powerSpectraPlaner(planerData, winsize,
currfftlength1024, fLow, fHigh);


%pressure focusing gain of transducer
winsizeDP = length(sampleData);      % Window size in DFT sample points
currSamRate = winsizeDP/(winsize*.000001);
st_freq = round(fLow*currfftlength1024/currSamRate) + 1;  %
10/14/2006, Convert frequency to DFT sample index
end_freq = round(fHigh*currfftlength1024/currSamRate) + 1;  %
10/14/2006, Convert frequency to DFT sample index
freqlength = end_freq – st_freq + 1;
 totalPFGT = zeros(1,freqlength);
 size(totalPFGT)
 for i = 1:freqlength;
    freqat = (st_freq –1 +i)*currSamRate/currfftlength1024;
   pfgt = a^2*pi*freqat/(rcurv*Cs);
     totalPFGT(1,i) =totalPFGT(1,i)+ pfgt;
 end
```

Appendix D

MATLAB Program to Load the RF Data

```
function [ rfdata ] = loadRFdata( FilePath, FileName )
% %UNTITLED2 Summary of this function goes here
% %   Detailed explanation goes here
% %import data
% UserInput = [];
% UserInput.filepath = filepath;
% UserInput.filename = filename;
%
% FileHeader = URIfileheader(UserInput);
%
% UserInput.FirstFrameN = start_frm;
% UserInput.SkipFrames = step_frm;
% UserInput.LastFrameN = end_frm;
%
%
% %load the RF data and vector header
% UserInput.FrameN = UserInput.FirstFrameN;
% VectorArray = URIload(UserInput, FileHeader);
% rfsz = size(VectorArray.RfData);
% numPlane = floor((end_frm – start_frm)/step_frm) + 1;
% % I must to initialize it first to save memory, otherwise, everytime
I do
% % Ref_RF3D(sliceNo,:,:) = RfDataFilt, the Ref_RF3D will have to open
an new
% % array with size+1 and then delete the old one.
% Ref_RF3D = zeros(numPlane, rfsz(1), rfsz(2));
% clear VectorArray;
%
% %%%%%%%%%%  for the case of many frames in one file
% for FrameN =
UserInput.FirstFrameN:UserInput.SkipFrames:UserInput.LastFrameN
%     UserInput.FrameN = FrameN;
%     VectorArray = URIload(UserInput, FileHeader);
%     if size(VectorArray.RfData,3)>1          % NOT useful
%         VectorArray_RfData =
VectorArray.RfData(:,:,UserInput.FrameN);
%     else
%         VectorArray_RfData = VectorArray.RfData;
%     end
%
%     % fft is only defined on double
%     RfDataFilt = double(VectorArray_RfData);  % don't do bandpass
filter


addpath(FilePath);
rfdata = xlsread(FileName);
%rfdata = dmlread(FileName);
% initialdata = xlsread(FileName);
% lengthdata = length(initialdata);
```

```
% rfdata = zeros(lengthdata,2);% 'int32'); ,'int32');
% %rfdata
%rfdata(:,1)=[];
% Vg = fft(rfdata);
% Vgstar = conj(Vg);
% powerSpectra = Vg.*Vgstar;
end
```

Appendix E

MATLAB Program to Calculate the Power Spectra of the HCT Cell Pellet

```
function [ avg_psd ] = powerSpectra( inputData, winsize,
currfftlength, fLow, fHigh, numFrame, alpha0, alpha1,
alpha2,rad1,rad2)
%powerSpectra takes the fft of rf data and squares it.
%currSamRate is Sampling frequency in MHz
%numFrame is the number of reference files (number of planes)
%numPtsPerLine is the sampled length of each Aline
%winsize_mm is the window length in mm
%currfftlength is the FFT length, generally used value is 1024
%fLow=low frequency in bandwidth in MHz
%fHigh=high frequency in bandwidth in MHz
% alpha0 and alpha1 and alpha2 are attenuation correction: attenuation
coeff: alpha0 + alpha1f + alpha2f^2
winsizeDP = length(inputData);      % Window size in DFT sample points
currSamRate = winsizeDP/(winsize*.000001);
st_freq = round(fLow*currfftlength/currSamRate) + 1;  % 10/14/2006,
Convert frequency to DFT sample index
end_freq = round(fHigh*currfftlength/currSamRate) + 1;  % 10/14/2006,
Convert frequency to DFT sample index
% st_freq = round(fLow*currfftlength/currSamRate); % 07/21/06, Convert
frequency to DFT sample index
% end_freq = round(fHigh*currfftlength/currSamRate); % 07/21/06,
Convert frequency to DFT sample index
zdistance = (rad2 - rad1)/2;
freqlength = end_freq - st_freq + 1;             % Bandwidth in DFT
sample index

% inputData
datalength=double(length(inputData));
avg_psd = zeros(freqlength,1);% 'int32'); ,'int32');
four_vR = zeros(datalength, 1);% 'int32'); , 'int32');
psd_v = zeros(datalength, 1);% 'int32'); , 'int32');

        for frmInd = 1:numFrame,
            currFrame = squeeze( inputData(:,:,frmInd));
            currFrame(:,1)=[];
            four_vR = fft(currFrame,currfftlength);   % no detrend
(only diff at 0 freq), rectangular win
            %four_vR
            psd_v = (four_vR.*conj(four_vR));  % Power spectrum of the
data no Hanning
%            size(psd_v)
            avg_psd(:,:)= avg_psd(:,:) + psd_v(st_freq:end_freq,:);
        end

    avg_psd = avg_psd / numFrame;  % see next line
    %avg_psd


%adjust for attenuation
```

```
  for i = 1:freqlength;
      freqat = (st_freq -1 +i)*currSamRate/currfftlength;
      attenCoeff= alpha0 + alpha1*(freqat/1000000)+alpha2*(freqat/
1000000)^2;
      correctionFactor = exp(4*attenCoeff*(rad1+zdistance));
       avg_psd(i,1) = avg_psd(i,1)*correctionFactor;
  end
% Write data to file

% fid=fopen(refFilename,'w');
% isFileWritten = fwrite(fid,avg_psd,'double');
% fclose(fid);

end
```

Appendix F

MATLAB Program to Calculate the Power Spectra of the Planar Reflector

```matlab
function [ avg_psd ] = powerSpectraPlaner( inputData, winsize,
currfftlength, fLow, fHigh)

%powerSpectra takes the fft of rf data and squares it.
%currSamRate is Sampling frequency in MHz
%numFrame is the number of reference files (number of planes)
%numPtsPerLine is the sampled length of each Aline
%winsize_mm is the window length in mm
%currfftlength is the FFT length, generally used value is 1024
%fLow=low frequency in bandwidth in MHz
%fHigh=high frequency in bandwidth in MHz
%
winsizeDP = length(inputData);     % Window size in DFT sample points
currSamRate = winsizeDP/(winsize*.000001);
st_freq = round(fLow*currfftlength/currSamRate) + 1;  % 10/14/2006,
Convert frequency to DFT sample index
end_freq = round(fHigh*currfftlength/currSamRate) + 1;  % 10/14/2006,
Convert frequency to DFT sample index
% st_freq = round(fLow*currfftlength/currSamRate); % 07/21/06, Convert
frequency to DFT sample index
% end_freq = round(fHigh*currfftlength/currSamRate); % 07/21/06,
Convert frequency to DFT sample index

freqlength = end_freq - st_freq + 1;               % Bandwidth in DFT
sample index
avg_psd = zeros(freqlength,1);% 'int32'); , 'int32');
%size(avg_psd)
inputData(:,1)=[];
datalength=double(length(inputData));
four_vR = zeros(datalength, 1);% 'int32'); , 'int32');
four_vR = fft(inputData,currfftlength);  % no detrend (only diff at 0
freq), rectangular win
psd_v = zeros(datalength, 1);% 'int32'); , 'int32');
psd_v = (four_vR.*conj(four_vR));  % Power spectrum of the data no
Hanning
%psd_v(:,1)=[];
%psd_v=squeeze(psd_v);
%size(psd_v)
avg_psd(:,:)= avg_psd(:,:)+ psd_v(st_freq:end_freq,:);


% Vg = fft(rfdata);
% Vgstar = conj(Vg);
% powerSpectra = Vg.*Vgstar;
%adjust for attenuation
% for i = 1:freqlength;
%     freqat = (st_freq -1 +i)*currSamRate/currfftlength;
%     avg_psd(i,:,:) = avg_psd(i,:,:)/saran_transCoeff(1540000,
1.601e6, .00025, freqat);
```

```
% end
% Write data to file

% fid=fopen(refFilename,'w');
% isFileWritten = fwrite(fid,avg_psd,'double');
% fclose(fid);


end
```

References:

[1] W. D. O'Brien, Jr. "A temporal view of soft tissue quantitative ultrasound," *Physics Procedia*, **70**, 1127-1130 (2015).

[2] E. J. Feleppa, J. Mamou, C. R. Porter and J. Machi. "Quantitative Ultrasound in Cancer Imaging", *Semin Oncol*. **38**, 136-150 (2011).

[3] G. Ghosal, J. Mamou and M. L. Oelze. "State of the art methods for estimating backscatter coefficients", in *Quantitative Ultrasound in Soft Tissue*. In: J. Mamou, M. L. Oelze (Eds.) Springer, New York, 3-19 (2013).

[4] J. Mamou, M. L. Oelze, W. D. O'Brien and J. F. Zachary. "Perspective on Biomedical Quantitative Ultrasound Imaging", *IEEE Signal Processing Magazine*, 112-116 (2006).

[5] E. J. Feleppa, A. Kalisz, J. B. Sokil-Melgar, F. L. Lizzi, T. Liu, A. L. Rosado, M. C. Shao, W. R. Fair, Y. Wang, M. S. Cookson, V. E. Reuter and W. D. W. Heston. "Typing of prostate tissue by ultrasonic spectrum analysis," *IEEE Trans. Ultrason Ferroelec Freq Contr*. **43**, 609-619 (1996).

[6] R. H. Silverman, R. Folberg, M. J. Rondeau, H. C. Boldt, H. O. Lloyd, X. Chen, F. L. Lizzi, T. A. Weingeist and D. J. Coleman, "Spectral parameter imaging for detection of prognostically significant histologic features in uveal melanoma," *Ultrasound Med Biol*. **29**, 951-959 (2003).

[7] F. L. Lizzi, D. L. King, M. C. Rorke, J. Hui, M. Ostromogilsky, M. M. Yaremko, E. J. Feleppa and P. Wai, "Comparison of theoretical scattering results and ultrasonic data from clinical liver examinations," *Ultrasound Med Biol*. **14**, 377-385 (1988)

[8] M. Yang, T. M. Krueger, J. G. Miller and M. R. Holland, "Characterization of anisotropic myocardial backscatter using spectral slope, intercept and midband fit parameters," *Ultrason Imaging*. **29**, 122-134 (2007).

[9] M. L. Oelze, W. D. O'Brien, J. P. Jr. Blue, J. F. Zachary, "Differentiation and characterization of rat mammary fibroadenomas and 4T1 mouse carcinomas using quantitative ultrasound imaging," *IEEE Trans Med Imaging*. **23**, 764-771 (2004).

[10] E. J. Feleppa, C. R. Porter, J. Ketterling, P. Lee, S. Dasgupata, S. Urban and A. Kalisz, et "Recent developments in tissue-type imaging (TTI) for planning and monitoring treatment of prostate cancer," *Ultrason Imaging*. **26**, 163-172 (2004).

[11] "HCT 116 Cell Line Human" *Sigma-Aldrich* Web. 30 Apr. 2017

[12] "Cancer Facts and Figures 2017," *American Cancer Society*. (2017)

[13] "Fact Sheets," *National Cancer Institute* (2017).

[14] A. Han, R. Abuhabsah, J. P. Blue Jr., S. Sarwate and W. D. O'Brien Jr., "Ultrasonic backscatter coefficient quantitative estimates from high-concentration Chinese hamster ovary cell pellet biophantoms," *J. Acoust. Soc. Am.*, **130**, 4138-4147 (2010).

[15] M. Teisseire, A. Han, R. Abuhabsah, J. P. Blue Jr., S. Sarwate and W. D. O'Brien Jr., "Ultrasonic backscatter coefficient quantitative estimates from Chinese hamster ovary cell pellet biophantoms," *J. Acoust. Soc. Am.*, **128**, 3175-3180 (2010).

[16] R. S. Cobbold, "Foundations of Biomedical Ultrasound," *New York: Oxford University Press, Inc.* (2006).

[17] T. L. Sazbo, "Diagnostic Ultrasound Imaging: Inside Out," *Academic Press*. **2** (2014).

[18] P. M. Morse and K. U. Ingard, "Theoretical Acoustics," *Princeton University Press*. (1986).

[19] R. A. Sigelmann and J. M. Reid, "Analysis and measurement of ultrasound backscattering from an ensemble of scatterers excited by sine wave bursts," *J. Acoust. Soc. Am.* **53**, 1351-1355 (1973).

[20] D. Jiang, H. Yang, J. K. V. Willson, J. Liang, L. E. Humphrey, E. Zborowska, D. Wang, J. Foster, R. Fan and M. G. Brattain, "Autocrine transforming growth factor α provides a growth advantage to malignant cells by facilitating re-entry into the cell cycle from suboptimal growth states," *J. Bio. Chem.*, **273**, 31471-31479 (1998).

[21] A. Rajput, I. D. San Martin, R. Rose, A. Beko, C. LeVea, E. Sharratt, R. Mazurchuk, R. M. Hoffman, M. G. Brattain and J. Wang, "Characterization of HCT116 human colon cancer cells in an orthotropic model," *Journal of Surgical Research*, **147**, 276-281 (2008).

[22] I. Chantret, A. Barbat, E. Dussaulx, M. G. Brattain, and A. Zweibaum. Epithelial polarity, villin expression, and enterocytic differentiation of cultured human colon carcinoma cells: a survey of twenty cell lines, *American Association for Cancer Research*, **48**, 1936-1942 (1988).

[23] A. Jemal, R. Siegel, E. Ward, T. Murray, J. Xu, C. Smigal and M. J. Thun, "Cancer statistics, 2006," *CA Cancer J Clin*. **52**, 106-130 (2006).

[24] R. J. Lavarello, W. R. Ridgway, S. S. Sarwarte and M. Oeleze, "Characterization of thyroid cancer in mouse models using high-frequency quantitative ultrasound techniques," *Ultrasound in Med. & Biol.* **39**, 2233-2341 (2013).

[25] M. L. Oelze, W. D. O'Brien Jr., J. P. Blue and J. F. Zachary, "Differentation and characterization of rat mammary fibroadenomas and 4T1 mouse carcinomas using quantitative ultrasound imaging," *IEEE Transactions on Medical Imaging*, **23**, 764-771 (2004).

[26] P. Muleki-Seya, R. Guillermine, J. Guglielmi, J. Chen, T. Pourcher, E. Konofagou and E. Franceschini, "High frequency quantitative ultrasound spectroscopy of excised canine livers and mouse tumors using the structure factor model," *IEEE Transactions on Ultrasonics, Ferroelectrics and Frequency Control*. **63**, 1335-1350 (2016).

[27] Picture from Chloe Verducci

[28] J. F Chen, J. A. Zagzebski and E. L. Madsen, "Tests of backscatter coefficient measurement using broadband pulses," *IEEE Trans. Ultrason Ferroelec Freq Contr*. **40**, 603-607 (1993).

[29] M. F. Insana, E. L. Madsen, T. J. Hall and J. A. Zagzebski, "Tests of the accuracy of a data reduction method for determination of acoustic backscatter coefficients," *Acoust. Soc. Am.* **79**, 1230-1236 (1996).

[30] E. L. Madsen, M. F. Insana and J. A. Zagzebski, "Method of data reduction for accurate determination of acoustic backscatter coefficients," *Acoust. Soc. Am.* **76**, 913-923 (1984).

[31] MATLAB. *version 8.5.0.197613 (R2015a)*. The MathWorks Inc., Natick, Massachusetts, 2015.

[32] G. Ghosal, A. C. Luchies, J. P. Blue, and M. L. Oelze, "Temperature dependent ultrasonic characterization of biological media," *J. Acoust. Soc. Am.*, **130**, 2203-2211(2011).

[33] T. J. Hall, E. L. Madsen, J. A. Zagzebski and E. J. Boote, "Accurate depth-independent determination of acoustic backscatter coefficients with focused transducers," *Acoustical Society of America*, **85**, 2410-2416 (1989).

[34] J. J. Anderson, M-T. Herd, M. R. King, A. Haak, Z. T. Hafez, J. Song, M. L. Oelze, E. L. Madsen, J. A. Zagzebski, W. D. O'Brien Jr. and T. J. Hall, "Interlaboratory comparison of backscatter coefficient estimates for tissue-mimicking phantoms", *Ultrason Imaging*, **32**, 48-64 (2010).